Bi-allelic variants in *IPO8* cause a connective tissue disorder associated with cardiovascular defects, skeletal abnormalities, and immune dysregulation

Alban Ziegler,[1,2,33] Rémi Duclaux-Loras,[3,33] Céline Revenu,[4,5,33] Fabienne Charbit-Henrion,[3,6,7] Bernadette Begue,[3] Karine Duroure,[4,5] Linda Grimaud,[2] Anne Laure Guihot,[2] Valérie Desquiret-Dumas,[1,2] Mohammed Zarhrate,[8] Nicolas Cagnard,[9] Emmanuel Mas,[10,11] Anne Breton,[10,11] Thomas Edouard,[12] Clarisse Billon,[13] Michael Frank,[13] Estelle Colin,[1] Guy Lenaers,[2] Daniel Henrion,[2] Stanislas Lyonnet,[14,15] Laurence Faivre,[16] Yves Alembik,[17] Anaïs Philippe,[17] Bruno Moulin,[18] Eyal Reinstein,[19,20] Shay Tzur,[21] Ruben Attali,[21] George McGillivray,[22] Susan M. White,[22] Lyndon Gallacher,[22,23] Kerstin Kutsche,[24] Pauline Schneeberger,[24] Katta M. Girisha,[25] Shalini S. Nayak,[25] Lynn Pais,[26] Reza Maroofian,[27] Aboulfazl Rad,[28] Barbara Vona,[28,29] Ehsan Ghayoor Karimiani,[30,31] Caroline Lekszas,[29] Thomas Haaf,[29] Ludovic Martin,[2,32] Frank Ruemmele,[3,6] Dominique Bonneau,[1,2] Nadine Cerf-Bensussan,[3] Filippo Del Bene,[4,5,*] and Marianna Parlato[3,*]

Summary

Dysregulated transforming growth factor TGF-β signaling underlies the pathogenesis of genetic disorders affecting the connective tissue such as Loeys-Dietz syndrome. Here, we report 12 individuals with bi-allelic loss-of-function variants in *IPO8* who presented with a syndromic association characterized by cardio-vascular anomalies, joint hyperlaxity, and various degree of dysmorphic features and developmental delay as well as immune dysregulation; the individuals were from nine unrelated families. Importin 8 belongs to the karyopherin family of nuclear transport receptors and was previously shown to mediate TGF-β-dependent SMADs trafficking to the nucleus *in vitro*. The important *in vivo* role of IPO8 in pSMAD nuclear translocation was demonstrated by CRISPR/Cas9-mediated inactivation in zebrafish. Consistent with IPO8's role in BMP/TGF-β signaling, *ipo8*$^{-/-}$ zebrafish presented mild to severe dorso-ventral patterning defects during early embryonic development. Moreover, *ipo8*$^{-/-}$ zebrafish displayed severe cardiovascular and skeletal defects that mirrored the human phenotype. Our work thus provides evidence that IPO8 plays a critical and non-redundant role in TGF-β signaling during development and reinforces the existing link between TGF-β signaling and connective tissue defects.

[1]Department of Biochemistry and Molecular Biology, CHU d'Angers, 49000 Angers, France; [2]University of Angers, MitoVasc, UMR CNRS 6015, INSERM 1083, 49933 Angers, France; [3]Université de Paris, Imagine Institute, Laboratory of Intestinal Immunity, INSERM, UMR1163, 75015 Paris, France; [4]Sorbonne Université, INSERM, CNRS, Institut de la Vision, 17 Rue Moreau, 75012 Paris, France; [5]Institut Curie, PSL Research University, INSERM U934, CNRS UMR3215, 75005 Paris, France; [6]Department of Pediatric Gastroenterology, Assistance Publique-Hôpitaux de Paris, Hôpital Necker-Enfants Malades, 75015 Paris, France; [7]Department of Molecular Genetics, Assistance Publique-Hôpitaux de Paris, Hôpital Necker-Enfants Malades, 75015 Paris, France; [8]Genomics Core Facility, Institut Imagine-Structure Federative de Recherche Necker, INSERM U1163 et INSERM US24/CNRS UMS3633, Paris Descartes Sorbonne Paris Cité University, 75015 Paris, France; [9]Bioinformatics Core Facility, INSERM-UMR 1163, Imagine Institute, 75015 Paris, France; [10]IRSD, Université de Toulouse, INSERM, INRA, ENVT, UPS, Toulouse 31300, France; [11]Centre de Référence des Maladies Rares Digestives, and Pediatric Clinical Research Unit, Toulouse Clinical Investigation Center INSERM U1436, Hôpital des Enfants, CHU de Toulouse, Toulouse 31300, France; [12]Reference Centre for Marfan Syndrome and Reference Centre on Rare Bone Diseases, Pediatric Clinical Research Unit, Children's Hospital, Toulouse University Hospital, RESTORE, INSERM UMR1301, 31300 Toulouse, France; [13]Centre de Génétique, Centre de Référence des Maladies Vasculaires Rares, Assistance Publique-Hôpitaux de Paris, Hôpital Européen Georges Pompidou, 75015 Paris, France; [14]Université de Paris, Imagine Institute, Laboratory of Embryology and Genetics of Malformations, INSERM UMR 1163, 75015 Paris, France; [15]Fédération de Génétique, Hôpital Necker-Enfants Malades, Assistance Publique Hôpitaux de Paris, 75015 Paris, France; [16]Centre de Référence Anomalies du Développement et Syndromes Malformatifs, FHU TRANSLAD, Hôpital d'Enfants, CHU Dijon, 21000 Dijon, France; [17]Département de Génétique Médicale, CHU de Hautepierre, 67200 Strasbourg, France; [18]Nephrology and Transplantation Department, Nouvel Hôpital Civil, Hôpitaux Universitaires de Strasbourg, 67200 Strasbourg, France; [19]Medical Genetics Institute, Meir Medical Center, Kfar-Saba 4428164, Israel; [20]Sackler Faculty of Medicine, Tel Aviv University, Tel Aviv 6997801, Israel; [21]Genomic Research Department, Emedgene Technologies, 67443 Tel Aviv, Israel; [22]Victorian Clinical Genetics Services, Murdoch Children's Research Institute, Parkville 3052, Melbourne, VIC, Australia; [23]Department of Paediatrics, The University of Melbourne, 3010 Parkville, Melbourne, VIC, Australia; [24]Institute of Human Genetics, University Medical Center Hamburg-Eppendorf, 20246 Hamburg, Germany; [25]Department of Medical Genetics, Kasturba Medical College, Manipal, Manipal Academy of Higher Education, Manipal 576104, India; [26]Broad Center for Mendelian Genomics, Program in Medical and Population Genetics, Broad Institute of Massachusetts Institute of Technology and Harvard, Cambridge, MA 02142, USA; [27]Department of Neuromuscular Disorders, Queen Square Institute of Neurology, University College London, WC1N 3BG London, UK; [28]Department of Otolaryngology–Head & Neck Surgery, Tübingen Hearing Research Centre, Eberhard Karls University of Tübingen, 72076 Tübingen, Germany; [29]Institute of Human Genetics, Julius Maximilians University Würzburg, 97074 Würzburg, Germany; [30]Molecular and Clinical Sciences Institute, St. George's, University of London, Cranmer Terrace London, SW17 ORE London, UK; [31]Innovative Medical Research Center, Mashhad Branch, Islamic Azdad University, Mashhad 9133736351, Iran; [32]Department of Dermatology, CHU d'Angers, 49000 Angers, France
[33]These authors contributed equally to this work
*Correspondence: filippo.del-bene@inserm.fr (F.D.B.), marianna.parlato@inserm.fr (M.P.)
https://doi.org/10.1016/j.ajhg.2021.04.020.

First isolated as a RanGTP-binding protein, importin 8 encoded by *IPO8* (MIM: 605600) was then identified as a member of the β-karyopherin family, the largest group of nuclear transport receptors.[1,2] Accordingly, *in vitro* studies have implicated importin 8 in cytoplasm-to-nucleus shuttling of a broad spectrum of cargos, including the signal recognition particle protein SRP19,[3] Argonaute-microRNAs complexes,[4,5] the c-Jun protein,[6] the NF-κB p65 subunit,[7] the eukaryotic translation initiation factor eIF4E,[8] and a set of receptor-activated mothers against decapentaplegic homolog (SMAD) transcription factors[9] that play a critical role downstream of the large family of tumor growth factor β (TGF-β) and bone morphogenetic protein (BMP) cytokines. In contrast, *in vivo* data on *IPO8* functions are lacking except for a report in *Drosophila* showing that Msk, the ortholog of mammalian importins 7 and 8 (which share 60% homology), mediates nuclear accumulation of phosphorylated MAD downstream of decapentaplegic, the homolog of mammalian BMP.[10] Msk inactivation was embryonically lethal, suggesting its key role in *Drosophila* development, but no link was clearly established with impairment of BMP signaling.[10]

Strikingly, the TGF-β/BMP cytokine family exerts pleiotropic functions during embryonic development, tissue homeostasis, and tissue repair as well as within the immune system.[11] Accordingly, dysregulation of TGF-β signaling is the cause of severe congenital disorders characterized by developmental defects with or without impaired immune regulation.[12] This is notably the case of Loeys-Dietz syndrome (LDS), which is caused by heterozygous loss-of-function (LOF) variants in *TGFBR1* (MIM: 190181), *TGFBR2* (MIM: 190182), *TGFB2* (MIM: 190220) or *TGFB3* (MIM: 190230), and *SMAD2* (MIM: 601366) or *SMAD3* (MIM: 603109);[13] of Shprintzen-Goldberg syndrome (SGS), which results from heterozygous variants in *SKI* (MIM: 182212), a negative regulator of the TGF-β signaling pathway;[14] and of Marfan syndrome (MFS) (MIM: 154700) caused by variants in *FBN1* (MIM: 134797), encoding fibrillin-1, the main component of extracellular matrix microfibrils that, in turn, scaffolds latent TGF-β. Thus, individuals with LDS, SGS, and MFS display systemic connective tissue disorders of variable expressivity, which notably affect the vascular tree and the skeleton, causing life-threatening arterial aneurysms, dysmorphic features, pectus deformity, scoliosis, and joint hyperlaxity.[14,15] In keeping with the immunoregulatory functions of TGF-β,[16,17] developmental defects of LDS have been associated with increased frequency of allergic manifestations[18] and a 10-fold increase in the risk of inflammatory bowel diseases (IBDs).[19] More recently, bi-allelic LOF variants in *TGFB1* (MIM: 190180) were identified as the cause of a severe syndrome combining very early-onset IBD and encephalopathy.[20]

Here, we report 12 individuals with bi-allelic pathogenic *IPO8* variants who displayed a complex syndrome reminiscent of LDS and SGS that variably combined cardiovascular, neurologic, skeletal and immunologic abnormalities along with dysmorphic features; the individuals are from nine unrelated families (Table 1, Figures 1 and S1). Affected individuals were recruited through an international collaborative effort facilitated by Genematcher.[21] All procedures were performed in accordance with the Helsinki Declaration and were approved by the ethics committees and the institutional review boards from each center. Sequencing (targeted/whole-exome sequencing and Sanger sequencing) was performed after obtaining informed written consent from all affected individuals or their legal guardians. Table 1 summarizes the main phenotypic features in the cohort. Seven individuals showed early-onset (before the age of 1 year for the youngest) dilatation of the ascending aorta. Individuals 1 and 2 (I-1 and I-2), the two oldest siblings (59 and 53 years old at the time of the first assessment, respectively) had diffuse arterial frailty with multiple aneurysms affecting the abdominal aorta, iliac, coronary, and renal arteries and, in I-1, the thoracic aorta (Figure 1A). Arterial tortuosity similar to that observed in LDS[22] was noted in four individuals. Recurrent spontaneous pneumothorax was noted in I-1 and I-2. Pulmonary emphysema was present in I-1 (Figure 1B) as well as in two younger individuals (I-5 and I-6). Facial dysmorphism was observed in ten individuals (Figure 1C, Table 1), while 11 had joint hyperlaxity complicated by multiple joint dislocations. All displayed skeletal features, including scoliosis (n = 9), pectus excavatum or carinatum (n = 6), arachnodactyly (n = 6), or pes planus or talipes equinovarus (n = 6) (Figures 1D–1F and S1). Eight individuals developed myopia complicated by retinal detachment for two of them and by early-onset cataract for two others, but none of them had lens dislocation. In line with a generalized connective tissue disorder, skin hyperextensibility and/or hernia were observed in 11 individuals (Figure 1G). Delayed motor milestone presumably consecutive to joint instability was observed in seven individuals; four of them also had mild (I-5, I-6, and I-8) or severe (I-7) intellectual disability. Predisposition to allergic or inflammatory diseases, which was previously documented in LDS,[18,19] was evidenced in six individuals (I-5, I-6, I-7, I-8, I-10, and I-12), some of whom also displayed immunological parameters consistent with impaired TGF-β signaling, including hyperIgE, hyperIgG, hypoIgA, and hypereosinophilia.

As detailed in Table 2, 11 variants were identified in the 12 individuals: seven as homozygous and four as compound heterozygous in *IPO8* (GenBank: NM_006390.3). This gene (25 exons, 24 introns) encodes a 1,037 amino acid protein with the β-importin N-terminal domain (22–102 aa) and a CSE1-like domain (202–441 aa) containing a RanGTPase-binding motif characteristic of β-importins (Figures 2A and 2B). Segregation of the variant within each family was analyzed by Sanger sequencing (Figure S2) whenever DNA was available (n = 8). They were all exceedingly rare (MAF < 0.01%), and only three were found in the gnomAD at a heterozygous state (Table 2).

Table 1. Clinical features of individuals carrying *IPO8* variants

	Family 1		Family 2		Family 3		Family 4	Family 5	Family 6	Family 7	Family 8	Family 9	Total
Individual	I-1	I-2	I-3	I-4	I-5	I-6	I-7	I-8	I-9	I-10	I-11	I-12	–
Sex	M	F	M	M	F	M	M	M	F	F	M	F	–
Age at last examination	62 years	62 years	1 year 8 months	2 years 2 months	16 years	15 years	9 years 6 months	13 years	22 years	33 years	7 years 6 months	26 years	–
Vascular abnormalities													
Dilatation of the ascending aorta	yes	yes	yes	no	yes	yes	yes	yes	yes	yes	yes	yes	11/12
Other abnormal great vessels	dilated and calcified iliac arteries, AAA	calcified coronary arteries, AAA, dilated iliac arteries	no	no	carotid artery tortuosity	carotid artery tortuosity	no	no	carotid artery tortuosity	no	no	internal carotid tortuosity and ectasia	6/12
Heart malformation	MVP	no	ASD, left atrium and ventricle mild dilatation	no	ASD, VSD	no	N/A	N/A	ASD	ASD, VSD	MVP	no	6/10
Ocular abnormalities													
Myopia	severe	severe	no	no	severe	no	no	severe	severe	mild	severe	severe	8/12
Retinal detachment	yes	yes	no	no	no	no	no	no	no	no	no	no	2/12
Dysmorphic features													
Proptosis	no	no	yes	no	no	yes	yes	no	yes	yes	yes	yes	7/12
Micrognathia	no	no	yes	yes	yes	yes	yes	no	yes	no	no	yes	7/12
Hypertelorism	no	no	yes	yes	yes	yes	yes	no	no	no	yes	no	6/12
Frontal bossing	no	no	yes	no	yes	yes	no	no	no	no	no	no	3/12
Ptosis	no	no	yes	no	no	no	yes	no	no	no	yes	no	3/12
Abnormal palate	no	no	cleft uvula	no	no	no	no	no	no	no	cleft uvula	no	2/12
Skeletal abnormalities													
Hyperlaxity	yes	yes	yes	yes	yes	yes	yes	yes	yes	yes	no	yes	11/12
Recurrent joint dislocations	yes	yes	yes	no	no	no	yes	no	yes	yes	no	yes	7/12
Pectus	no	no	carinatum	carinatum	excavatum	excavatum	no	no	excavatum	no	carinatum	no	6/12
Scoliosis	yes	yes	no	no	yes	yes	yes	yes	yes	yes	yes	no	9/12
Arachnodactyly	no	no	yes	yes	yes	yes	no	no	yes	no	yes	no	6/12

(*Continued on next page*)

Table 1. ***Continued***

	Family 1		Family 2		Family 3		Family 4	Family 5	Family 6	Family 7	Family 8	Family 9	Total
Feet malposition	no	no	yes	yes	no	no	no	yes	yes	yes	yes	no	6/12
Connective tissue abnormalities													
Skin hyperextensibility	no	no	yes	yes	yes	yes	no	yes	no	yes	yes	yes	8/12
Hernia	umbilical hernia	spigelian and umbilical hernia	inguinal, umbilical, diaphragmatic hernia	umbilical hernia	umbilical and inguinal hernia	umbilical and inguinal hernia	umbilical and inguinal hernia	umbilical hernia	no	umbilical and abdominal hernia	umbilical hernia	umbilical and abdominal hernia	11/12
Developmental delay/intellectual disability	no	no	yes	yes	yes	yes	yes	yes	no	no	yes	no	7/12
Immunological abnormalities													
HyperIgE	N/A	N/A	N/A	N/A	yes	yes	N/A	yes	N/A	N/A	N/A	N/A	3/3
HyperIgG	N/A	N/A	N/A	N/A	yes	yes	N/A	yes	N/A	N/A	N/A	N/A	3/3
HypoIgA	N/A	N/A	N/A	N/A	yes	yes	N/A	yes	N/A	N/A	no	N/A	3/4
Hypereosinophilia	mild	N/A	N/A	N/A	yes	yes	N/A	yes	N/A	N/A	no	N/A	4/5
Intestinal inflammation	no	no	no	no	severe colitis	celiac disease/ gastritis	no	dysimmune gastroenterocolitis	no	no	chronic gastritis and duodenitis	celiac disease	5/12
Allergic symptoms	no	no	no	no	asthma, eczema	asthma, eczema	asthma	eczema, rhinoconjunctivitis	no	asthma	no	drug allergies	6/12
Urogenital/kidney anomalies	large cortical cyst	ischemic nephropathy	ureterohydronephrosis	no	pyelo-ureteral duplication	no	N/A	ureterohydronephrosis	no	no	hydronephrosis	no	6/11

AAA, ascending aortic aneurysm; ASD, atrial septal defect; MVP, mitral valve prolapse; VSD, ventricular septal defect; N/A, not available. Severe myopia was defined as of −6.00 diopters or greater.

Figure 1. Clinical features of affected individuals
(A) CT scan showing dilated aortic root and thoracic aorta (TA), calcified asymmetric large femoral arteries (FA), calcified and dilated abdominal aorta (AA), and large renal cyst (white star) in individual 1.
(B) CT scan showing emphysema of the apex of the left lung in individual 1.
(C) Proptosis, micrognathia, and hypertelorism in individuals 3, 4, and 10.
(D) X-ray showing scoliosis in individuals 1 and 7.
(E) Arachnodactyly in individuals 3 and 7.
(F) Hyperlaxity of small and large joints in individuals 10 and 7.
(G) Pes planus and talipes equinovarus in individuals 10 and 3, respectively.
(H) Skin hyperextensibility in individuals 4, 7, and 10 and umbilical hernia in individual 5.

Out of the seven homozygous variants, four were likely LOF variants (three nonsense, c.2407C>T [p.Arg803*], c.82C>T [p.Gln28*], and c.2129C>G [p.Ser710*], and one frameshift c.728delC [p.Pro243Leufs*27]), one was a splicing variant (c.2695+3_2695+7delAAAGT), and two were missense (c.262G>A [p.Asp88Asn] and c.2500C>T [p.Arg834Trp]). The compound heterozygous variants were frameshift variants leading to a premature stop codon (c.2279delT [p.Leu760ProfsTer10] and c.1538delC [p.Pro 513Leufs*13]) in *trans* with a splicing (c.2900−1G>A) and a missense variant (c.2245T>C [p.Cys749Arg]), respectively. Both, c.2695+3_2695+7delAAAGT and c.2900−1 G>A variants were predicted to impact the splicing according to SpliceAI.[23] Although the lack of available biospecimens or DNA from I-10 (family 7) prevented assessment of the splicing variant C.2900−1 G>A, analysis of the c.2695+3_2695+7delAAAGT variant by minigene assay demonstrated that it resulted in exon 22 skipping and activation of a cryptic splicing site (Figure S3). The *IPO8* missense variants, namely p.Asp88Asn, p.Cys749Arg, and p.Arg834Trp, affected highly conserved residues among IPO8 orthologs and were predicted to be damaging by several *in silico* tools, including CADD score (Figure 2B).

The impact of variants on protein level was evaluated by immunoblot analysis of protein lysates from primary cells, either fibroblasts or Epstein-Barr virus-immortalized B cell lines (EBV-B cells). A striking reduction of IPO8 level was observed in the four individuals who could be tested, including I-2 and I-9, who carried homozygous missense variants (Figure 2C). The overlap of clinical features

Table 2. Characteristics of *IPO8* variants identified by next-generation sequencing in affected individuals

Individual	Chromosome position (Hg19-GRCh37) chr12	cDNA change (GenBank: NM_006390.3)	Amino acid change	SIFT	PolyPhen	DANN	CADD	Mutation Taster	Allele frequency gnomAD
1–2	g.30837296C>T	c.262G>A	p.Asp88Asn	damaging	probably damaging	0.9989	25.3	disease causing	not observed
3–4	g.30792531G>A	c.2407C>T	p.Arg803*	N/A	N/A	0.9979	36	disease causing	3.98E−6, no homozygotes
5–6	g.30848500G>A	c.82C>T	p.Gln28*	N/A	N/A	0.9984	39	disease causing	not observed
7	g.30789909_30789913del	c.2695+3_2695+7delAAAGT	N/A	N/A	N/A	N/A	22.8	disease causing	not observed
8	g.30816479del	c.1538delC	p.Pro513Leufs* 13	N/A	N/A	N/A	33	disease causing	not observed
	g.30802094A>G	c.2245T>C	p.Cys749Arg	damaging	probably damaging	0.9978	28.4	disease causing	not observed
9	g.30790111G>A	c.2500C>T	p.Arg834Trp	damaging	probably damaging	0.9993	32	disease causing	4.03E−6, no homozygotes
10	g.30784946C>T	c.2900−1G>A	N/A	N/A	N/A	0.9935	34	disease causing	not observed
	g.30792659del	c.2279delT	p.Leu760Profs* 10	N/A	N/A	N/A	33	disease causing	1.06E−5, no homozygotes
11	g. 30829433del	c.728del	p.Pro243Leufs* 27	N/A	N/A	N/A	33	disease causing	not observed
12	g.30805169G>C	c.2129C>G	p.Ser710*	N/A	N/A	0.9962	38	disease causing	not observed

between all the affected individuals and the rarity or absence of the identified *IPO8* variants in population databases, including LOF variants and three missense variants impairing protein level and/or with predicted damaging effect on protein function, strongly supported IPO8 deficiency as disease causing in all the 12 individuals.

We next assessed how *ipo8* disruption might affect development by using a zebrafish model and focused attention on early dorso-ventral patterning defects that are a telltale sign of altered TGF-β/BMP signaling, as well as on skeletal and cardiovascular defects that were the main clinical hallmarks in the cohort. The zebrafish genome encodes one single *ipo8* ortholog with 72% identity and 85% similarity with human IPO8. IPO8 mutants were generated via CRISPR/Cas9 genome editing and two RNA guides simultaneously. The selected fish line carried both one insertion and two deletions (indels) in exon 4 that overall resulted in alternative translation from amino acid 125 and introduction of an early stop codon after amino acid 136 (Figure 3A). Zygotic mutants derived from the incross of two heterozygous parents ($ipo8^{idv1/+}$ or simply $ipo8^{+/-}$) did not develop any obvious phenotype and could be grown to adulthood, a result in keeping with the fact that maternal factors stored as mRNAs and proteins in the egg can compensate for zygotic loss of function during embryonic stages of zebrafish.[24,25] In order to obtain maternal-zygotic mutants (MZ $ipo8^{-/-}$, here referred to simply as $ipo8^{-/-}$) that lacked wild-type (WT) ipo8 provided in the egg by the mother, we incrossed homozygous *ipo8* zygotic mutant adults. Their homozygous WT siblings were incrossed as controls. At 10 h post fertilization (hpf) (bud stage), $ipo8^{-/-}$ MZ embryos appeared ovoid rather than round (Figure 3B). Moreover, during the following early somite stages, their tail bud failed to extend around the yolk but extended off prematurely, generating elongated, pear-shaped embryos (86% of 36 embryos from 3 clutches). These early morphological changes correlated with increased death rate that varied between 20% to 100% of the embryos per clutch. As development proceeded, a range of tail elongation defects became apparent, from embryos displaying an entirely normal or only partially absent ventral tail fin to embryos with a strongly twisted body axis resembling a snail shell-like trunk (Figure 3C). In addition, at 3 days post fertilization (dpf), most embryos (81% of 83 larvae from 6 clutches) developed heart edemas (as highlighted by arrows in Figure 3C). Morphological changes were strongly pronounced in the tail region, while anterior parts appeared comparatively normal with well-developed eyes and visible midbrain-hindbrain boundaries. These features are typical of dorsalized zebrafish mutants that result from mutations affecting the specification of ventral regions.[26] To quantify the dorsalization phenotypic spectrum of the $ipo8^{-/-}$ mutants, we evaluated each analyzed clutch at 24 hpf and divided the phenotypes into five severity classes as previously described.[26] A normal phenotype was observed in 96.5% of WT embryos but only 4.5% of $ipo8^{-/-}$ embryos, which displayed a whole spectrum of dorsalization phenotypes (Figures 3D and 3E).

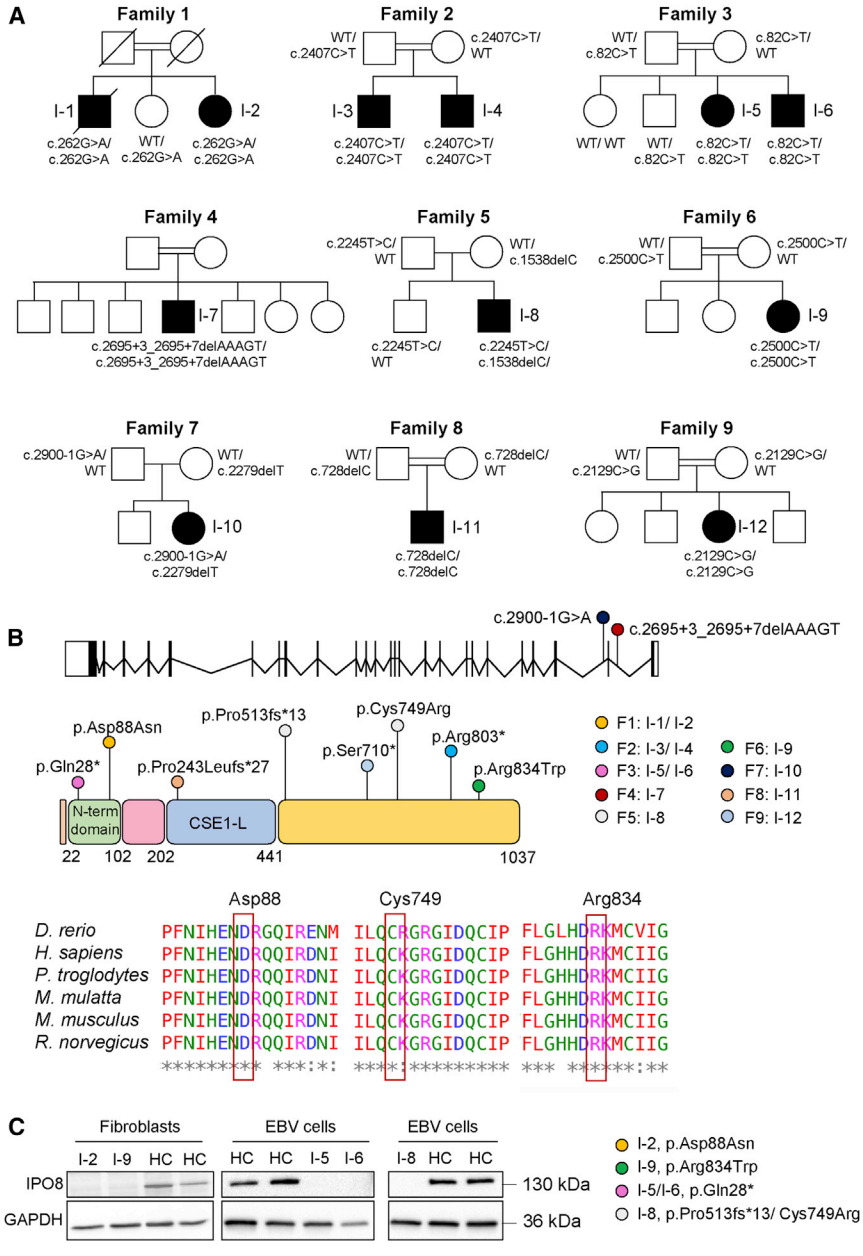

Figure 2. Molecular features of identified variants

(A) Pedigrees of families 1–9.

(B) Schematic representation of *IPO8* gene (25 exons, 24 introns) and importin 8 protein (1,037 amino acids), which features the importin N-terminal domain and the CSE1-like domain, containing tandem HEAT repeats and a RanGTP-binding motif. *IPO8* variants identified in this study as well as their location are shown. Protein sequence alignments of IPO8 orthologs are provided for each affected residue.

(C) Importin 8 expression in fibroblasts or EBV cells derived from individuals 2, 5, 6, 8, and 9. GAPDH served as loading control.

To dissect these morphological defects at the molecular level, we performed whole-mount *in situ* hybridization analysis to reveal mRNA expression of early patterning genes in embryos (Figure S4). *Ntl* showed a shorter and broader expression pattern indicating defects in axial mesoderm elongation (Figure S4A). *Gata1* showed reduced expression limited to the posterior side, indicating ventral mesoderm specification defects (Figure S4B). In addition, the paraxial mesoderm marker *myoD* showed a shorter and broader pattern, underlying defects in convergent-extension gastrulation movements (Figure S4C). Overall, these defects in *ipo8* mutants appeared comparable to those reported in zebrafish dorsalized mutants, which affect members of BMP and TGF-β signaling (e.g., *bmp2*, *bmp7*, *alk8*, and *smad5*).[27,28] To investigate skeletal defects in the *ipo8*$^{-/-}$ zebrafish model, we analyzed expression of the transcription factor sox9a, a marker of chondrogenic precursor development (Figure S4D). Shorter trabeculae of the neurocranium were observed in mutant embryos by 2 dpf. In the tail region, *sox9a* expression was strongly reduced or appeared in irregular patches along the spinal cord axis, consistent with defects in vertebrae formation. Heart and vessel morphologies were analyzed after crossing the *ipo8* mutant line with a transgenic line expressing a reporter fluorescently labeling blood vessels in living embryos (*Tg*(*kdrl:Hsa.HRAS-mCherry*)). Analysis at 2 dpf revealed severe defects in heart chamber formation and atrial and ventricular chambers were less or not delimited in *ipo8*$^{-/-}$ mutants (Figure 4A). *Ipo8*$^{-/-}$ mutants also exhibited arterio-venous malformations in the head and over 70% of mutant embryos in 5 independent clutches showed abnormal arterio-venous connections in the dorsal midline junction and poorly differentiated central arteries that appeared irregular, thin, and poorly lumenized (Figure 4B). By 3 dpf, various severe cardiovascular defects were observed in mutant embryos, including heart edema and, in the subset of embryos with mild tail morphological defects (normal or C1 class in Figure 3D), various blood vessel patterning abnormalities that resulted in the absence of blood circulation or abnormal blood flow in the tail region (e.g., looping or clogging, Figure 4C).

Putative defects in TGF-β/BMP signaling in the *ipo8*$^{-/-}$ mutants were next investigated with an antibody specific for pSmad1/5/9. This antibody revealed the expected ventral to dorsal gradient of pSmad1/5/9 detected in WT gastrulating embryos with nuclear localization in the ventral part. In *ipo8*$^{-/-}$ embryos, nuclear localization of

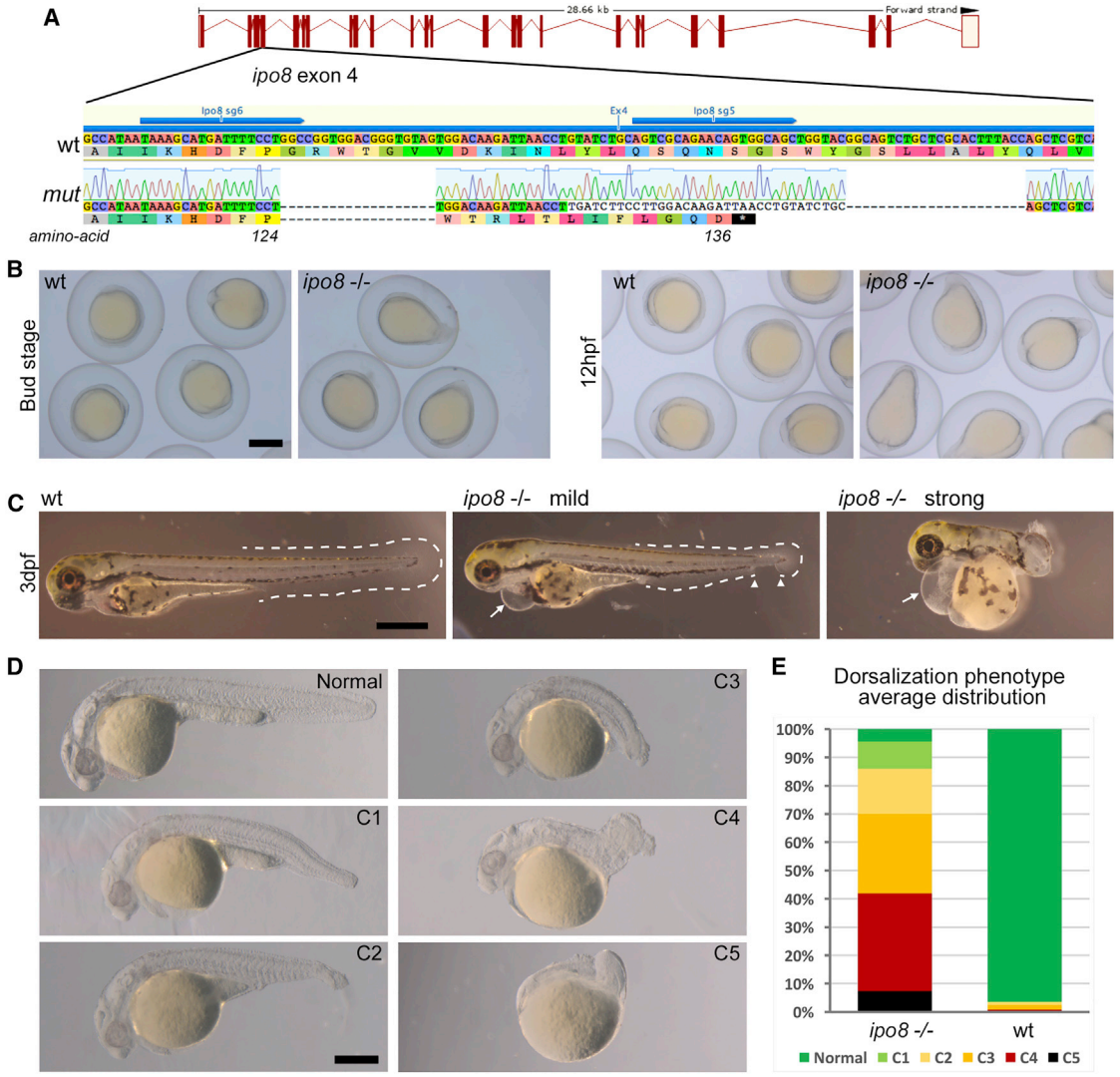

Figure 3. Zebrafish *ipo8* mutants show a range of dorsalization phenotypes

(A) Schematics of CRISPR/Cas9-mediated gene disruption at the *ipo8* genomic locus. The sgRNAs (sg5 and sg6, blue arrows) targeted exon 4. Compared to the wild-type (WT) sequence, the mutated allele from the founder fish (*mut*) displayed two deletions of 18 and 22 bases and an insertion of 34 bp generating a frameshift from amino acid 124 and a premature STOP codon after 136 amino acids.

(B) Bright field pictures of bud (10 hpf) and early somite stages (12 hpf) embryos showing the elongating shape of the $ipo8^{-/-}$ embryos compared to WT controls. Scale bar represents 500 μm.

(C) Bright field pictures of 3 dpf larvae presenting the variable penetrance of the $ipo8^{-/-}$ phenotype (mild and strong) compared to WT controls. The tail fin is circled with dashed lines when visible. Gaps are highlighted by arrowheads. Arrows point at heart edema. Scale bar represents 200 μm.

(D) Nomarski pictures depicting the different classes of the dorsalization phenotype at 24 hpf as described in Mullins et al.[26] (from severe C5 to mild C1) in the $ipo8^{-/-}$ mutants compared to the normal phenotype of a WT embryo. Scale bar represents 200 μm.

(E) Quantification of the distribution of the dorsalization classes in $ipo8^{-/-}$ mutants (5 clutches, n = 903) compared to WT clutches (4 WT clutches, n = 503). Average values in $ipo8^{-/-}$ mutants were 7.3% C5, 34.6% C4, 28.0% C3, 16.0% C2, 9.6% C1, and 4.5% normal, and average values in WT controls were 0% C5, 0.8% C4, 1.6% C3, 1.1% C2, 0% C1, and 96.5% normal.

pSmad was significantly reduced (Figures 5A and 5B). In contrast and in keeping with a defect in pSMAD translocation in $ipo8^{-/-}$ embryos, the pSMAD signal was detected in the cytoplasm and at membranes, as shown by its colocalization with phalloidin at cell outlines.

To further demonstrate the role of *ipo8* in TGF-β/BMP signaling during development, we compared the transcriptomes of WT and $ipo8^{-/-}$ embryos at two different time points during early embryogenesis (13 and 24 hpf) (Figure 5C). We chose these early developmental stages to avoid secondary effects deriving from abnormalities developing later on. *Ipo8* itself, as expected, was significantly downregulated in $ipo8^{-/-}$ fish (Figure S5A). Principal-component analysis (PCA) showed close clustering of biological replicates and a clear segregation of the $ipo8^{-/-}$ samples from WT samples both at 13 and 24 hpf (Figure S5B). Genes differentially regulated between the $ipo8^{-/-}$ and WT embryos (adjusted p value < 0.01) were analyzed by pathway enrichment analysis (Figure 5C). Strikingly, genes differentially regulated upon ipo8

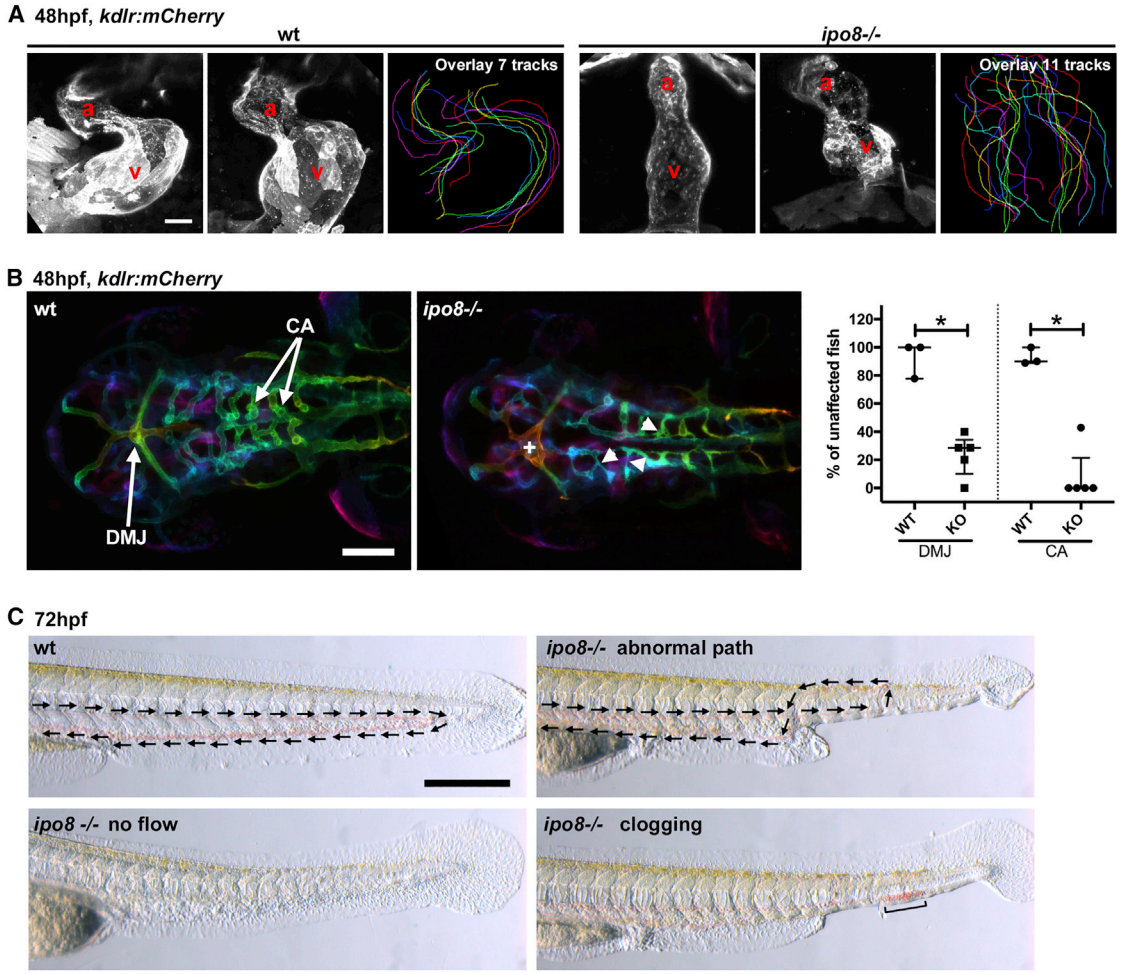

Figure 4. ***Ipo8*** **deficiency causes cardiovascular defects in zebrafish**

(A) Defects in heart chamber formation exemplified by two maximal projections of confocal *Z* stacks of the hearts of WT and *ipo8*$^{-/-}$ 48 hpf embryos carrying the kdrl:mCherry transgene to label endothelial cells. For each line, the third panel shows the overlays of the outlines of the 7 (WT) and 11 *(ipo8*$^{-/-}$*)* analyzed hearts. a, atrium; v, ventricle. Scale bar represents 30 μm.

(B) Maximal projections of depth color-coded confocal *Z* stacks of the head vessels of WT and *ipo8*$^{-/-}$ embryos at 48 hpf, and quantifications of the percentage of fish showing dorsal midline junction (DMJ) defects and central arteries (CA) differentiation defects. Twenty-three WT and 30 *ipo8*$^{-/-}$ embryos from 3 and 5 clutches, respectively, were analyzed. Median and IQR are shown. p values were calculated by Mann Whitney test (*$p < 0.05$). +, abnormal DMJ; arrowheads, abnormal CA. Scale bar represents 100 μm.

(C) Maximal projections of time-lapses of Nomarsky imaging of the tails of 3 dpf larvae highlighting absence of blood circulation (no flow) or defects in blood vessel patterning (abnormal path and clogging) in *ipo8*$^{-/-}$ mutants. Arrows indicate flow direction. Scale bar represents 200 μm.

depletion encoded multiple components of the TGF-β/BMP pathway as well as genes involved in angiotensin/angiogenesis pathways. Notably, expression of *smad7*, one of the direct transcriptional targets of the TGF-β/BMP pathway, was strongly decreased in *ipo8*$^{-/-}$ embryos compared to WT at both 13 and 24 hpf, compatible with lack of translocation to the nucleus and, as a consequence, impaired downstream activation of SMAD-dependent transcription.

Overall, our zebrafish model demonstrates that importin 8 plays a critical role during the early stage of development by controlling pSmad nuclear translocation and downstream TGF-β/BMP-dependent transcription. Because homozygous *ipo8*$^{-/-}$ embryos born from heterozygous parents were normal, and because the abnormal phenotype was observed only in MZ mutant embryos, it is likely that Ipo8 is not essential after the initial embryogenesis occurs. This may be due to genetic compensation[29] or simply to Ipo8 function's being redundant with that of a paralog. We cannot, however, exclude subtler cellular/organ phenotypes that may occur later in development or in adult animals and have not been characterized in this study. Importantly, data in the zebrafish model support a causative role of IPO8 deficiency in the vascular and skeleton defects observed in all affected individuals. While our results indicate a role for Ipo8 via the nuclear translocation of phosphorylated SMAD proteins, future investigation remains necessary to define whether and how the role of IPO8 in the translocation of other putative cargoes[3–7] (see above) may participate in the phenotypic features of IPO8 deficiency.

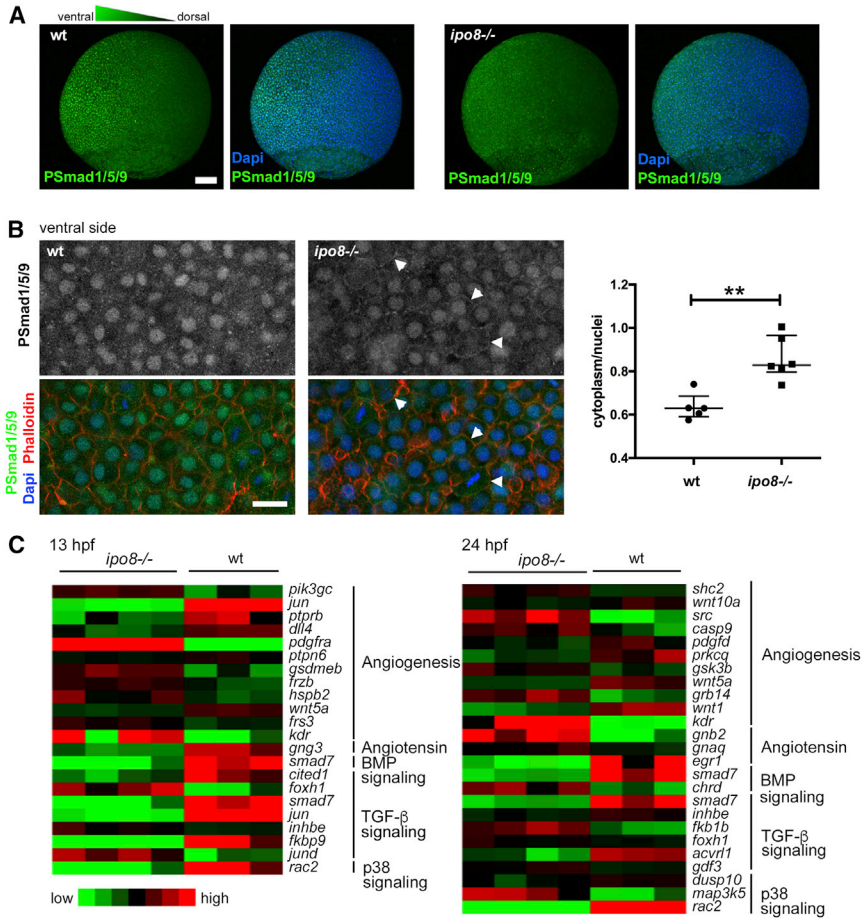

Figure 5. pSMAD nuclear translocation defects in *ipo8*$^{-/-}$ embryos highlight impaired TGF-β/BMP signaling

(A) Maximal projections of confocal *Z* stacks of WT and *ipo8*$^{-/-}$ embryos labeled for pSmad1/5/9 (green) and DAPI (blue) showing well-defined ventral to dorsal gradient of pSmad5 in WT gastrulating zebrafish embryos (left panel) but not in the *ipo8*$^{-/-}$ embryos (right panel). Scale bar represents 100 μm.

(B) Confocal images of the ventral sides of WT and *ipo8*$^{-/-}$ embryos labeled for pSmad1/5/9 (green), phalloidin (red), and DAPI (blue). Arrowheads highlight the membrane localization of the pSmad staining in the *ipo8*$^{-/-}$ mutants. Scale bar represents 20 μm. Dot plots representative of three experiments show quantifications of the ratio of pSmad1/5/9 cytoplasmic signal over nuclear signal; 5 WT and 6 *ipo8*$^{-/-}$ embryos were analyzed. Median and IQR are shown. p values were calculated by Mann Whitney test (**$p < 0.01$).

(C) Heatmaps of differentially expressed genes between WT and *ipo8*$^{-/-}$ embryos at 13 and 24 hpf. Three to four biological replicates are shown per group. The top enriched gene ontology term for biological process is highlighted for each cluster.

In summary, we have identified *IPO8* deficiency as the cause of a previously uncharacterized syndrome that is inherited in an autosomal-recessive pattern. This syndrome is characterized by deregulation of TGF-β signaling pathway and overlaps clinically with other TGF-β signalopathies: MFS, LDS, and SGS as depicted in Figure S6 and Table S1. Common features observed in IPO8 individuals and shared with LDS, MFS, and SGS include cardiovascular anomalies with notably strong predisposition for ascending aorta aneurysm and facial and skeletal anomalies (Table S1). Other less recurrent manifestations displayed by IPO8-deficient individuals were immune dysregulation and allergic diseases, which have also been reported in a subset of LDS-affected individuals,[30] and developmental delay that was observed in SGS.[14] The accompanying article by Van Gucht et al.[31] in this issue of *The American Journal of Human Genetics* reports largely overlapping developmental abnormalities in seven additional *IPO8*-deficient individuals.[31] Their data showing that the loss of ipo8 causes severe early-onset thoracic aortic aneurysm in a mouse model supports the causative role of the gene defect in the most severe manifestation of the disease and complements our demonstration that IPO8 plays a crucial role in TGF-β-dependent organogenesis and in cardio-vascular development in the zebrafish model. Overall, the identification of IPO8 deficiency as cause of TGF-β signalopathy stresses the essential functions of this pathway in development, patterning, and homeostasis of the affected tissues.

Data and code availability

The *IPO8* variants were submitted to ClinVar (https://www.ncbi.nlm.nih.gov/clinvar/) (GenBank: NM_006390.3; accession numbers SCV001571677, SCV001571678, SCV001571679, SCV001571680, SCV001571681, SCV001571682, SCV001571683, SCV001571684, SCV001571685, SCV001571686, and SCV001571687). The WES datasets supporting this study have not been deposited in a public repository because of ethical restriction but are available from the corresponding author on request.

Supplemental information

Supplemental information can be found online at https://doi.org/10.1016/j.ajhg.2021.04.020.

Acknowledgments

We are grateful to the families who participated in this work. We thank Nicole Van Bergen, MCRI, for performing the confirmatory Sanger sequencing in individual 10. This work was supported by

the Agence Nationale de la Recherche under "Investissements d'avenir" program (ANR-10-IAHU-01), institutional grants from INSERM, the European grant ERC-2013-AdG-339407-IMMUNOBIOTA, and grants from Fondation Princesse Grace and "Fondation Maladies Rares" (to N.C.B.); by institutional grants from the CNRS and the University of Angers (to D.B.); by intramural funding (*f*ortüne) at the University of Tübingen (2545-1-0) and the Ministry of Science, Research and Art Baden-Württemberg (to B.V.); and by the Programme Investissements d'Avenir IHU FOReSIGHT (ANR-18-IAHU-01) (to F.D.B.). C.R. was supported by an EU Horizon 2020 Marie Skłodowska-Curie Action fellowship (H2020-MSCA-IF-2014 #661527). K.M.G. and K.K. are jointly funded by the Indian Council of Medical Research (file no. 5/7/1508/2016 to K.M.G.) and the Federal Ministry of Education and Research (01DQ17003 to K.K.). Sequencing and analysis for individual 10 were provided by the Broad Institute of MIT and Harvard Center for Mendelian Genomics (Broad CMG) and was funded by the National Human Genome Research Institute, the National Eye Institute, and the National Heart, Lung, and Blood Institute grant UM1 HG008900 and in part by National Human Genome Research Institute grant R01 HG009141. Funding for the UDP-Vic was provided by philanthropic donation and the Murdoch Children's Research Institute. The research conducted at the Murdoch Children's Research Institute was supported by the Victorian Government's Operational Infrastructure Support Program, the Harbig Family Foundation, and The Royal Children's Hospital Foundation.

Declaration of interests

The authors declare no competing interests.

Received: January 24, 2021
Accepted: April 23, 2021
Published: May 18, 2021

Web resources

CADD, https://cadd.gs.washington.edu/
GenBank, https://www.ncbi.nlm.nih.gov/genbank/
GeneMatcher, https://genematcher.org/
gnomAD, https://gnomad.broadinstitute.org/
Mutation Taster, http://www.mutationtaster.org/
OMIM, https://omim.org
PolyPhen2, http://genetics.bwh.harvard.edu/pph2/
SIFT, https://sift.bii.a-star.edu.sg/

References

1. Görlich, D., Dabrowski, M., Bischoff, F.R., Kutay, U., Bork, P., Hartmann, E., Prehn, S., and Izaurralde, E. (1997). A novel class of RanGTP binding proteins. J. Cell Biol. *138*, 65–80.
2. Stewart, M. (2007). Molecular mechanism of the nuclear protein import cycle. Nat. Rev. Mol. Cell Biol. *8*, 195–208.
3. Dean, K.A., von Ahsen, O., Görlich, D., and Fried, H.M. (2001). Signal recognition particle protein 19 is imported into the nucleus by importin 8 (RanBP8) and transportin. J. Cell Sci. *114*, 3479–3485.
4. Wei, Y., Li, L., Wang, D., Zhang, C.-Y., and Zen, K. (2014). Importin 8 regulates the transport of mature microRNAs into the cell nucleus. J. Biol. Chem. *289*, 10270–10275.
5. Weinmann, L., Höck, J., Ivacevic, T., Ohrt, T., Mütze, J., Schwille, P., Kremmer, E., Benes, V., Urlaub, H., and Meister, G. (2009). Importin 8 is a gene silencing factor that targets argonaute proteins to distinct mRNAs. Cell *136*, 496–507.
6. Schreck, I., Al-Rawi, M., Mingot, J.-M., Scholl, C., Diefenbacher, M.E., O'Donnell, P., Bohmann, D., and Weiss, C. (2011). c-Jun localizes to the nucleus independent of its phosphorylation by and interaction with JNK and vice versa promotes nuclear accumulation of JNK. Biochem. Biophys. Res. Commun. *407*, 735–740.
7. Liang, P., Zhang, H., Wang, G., Li, S., Cong, S., Luo, Y., and Zhang, B. (2013). KPNB1, XPO7 and IPO8 mediate the translocation ofNF-κB/p65 into the nucleus. Traffic *14*, 1132–1143.
8. Volpon, L., Culjkovic-Kraljacic, B., Osborne, M.J., Ramteke, A., Sun, Q., Niesman, A., Chook, Y.M., and Borden, K.L.B. (2016). Importin 8 mediates m7G cap-sensitive nuclear import of the eukaryotic translation initiation factor eIF4E. Proc. Natl. Acad. Sci. USA *113*, 5263–5268.
9. Yao, X., Chen, X., Cottonham, C., and Xu, L. (2008). Preferential utilization of Imp7/8 in nuclear import of Smads. J. Biol. Chem. *283*, 22867–22874.
10. Xu, L., Yao, X., Chen, X., Lu, P., Zhang, B., and Ip, Y.T. (2007). Msk is required for nuclear import of TGF-β/BMP-activated Smads. J. Cell Biol. *178*, 981–994.
11. David, C.J., and Massagué, J. (2018). Contextual determinants of TGFβ action in development, immunity and cancer. Nat. Rev. Mol. Cell Biol. *19*, 419–435.
12. MacFarlane, E.G., Haupt, J., Dietz, H.C., and Shore, E.M. (2017). TGF-β Family Signaling in Connective Tissue and Skeletal Diseases. Cold Spring Harb. Perspect. Biol. *9*, a022269.
13. Schepers, D., Tortora, G., Morisaki, H., MacCarrick, G., Lindsay, M., Liang, D., Mehta, S.G., Hague, J., Verhagen, J., van de Laar, I., et al. (2018). A mutation update on the LDS-associated genes TGFB2/3 and SMAD2/3. Hum. Mutat. *39*, 621–634.
14. Doyle, A.J., Doyle, J.J., Bessling, S.L., Maragh, S., Lindsay, M.E., Schepers, D., Gillis, E., Mortier, G., Homfray, T., Sauls, K., et al. (2012). Mutations in the TGF-β repressor SKI cause Shprintzen-Goldberg syndrome with aortic aneurysm. Nat. Genet. *44*, 1249–1254.
15. Loeys, B.L., Chen, J., Neptune, E.R., Judge, D.P., Podowski, M., Holm, T., Meyers, J., Leitch, C.C., Katsanis, N., Sharifi, N., et al. (2005). A syndrome of altered cardiovascular, craniofacial, neurocognitive and skeletal development caused by mutations in TGFBR1 or TGFBR2. Nat. Genet. *37*, 275–281.
16. Chen, W., and Ten Dijke, P. (2016). Immunoregulation by members of the TGFβ superfamily. Nat. Rev. Immunol. *16*, 723–740.
17. Kelly, A., Houston, S.A., Sherwood, E., Casulli, J., and Travis, M.A. (2017). Regulation of Innate and Adaptive Immunity by TGFβ. Adv. Immunol. *134*, 137–233.
18. Frischmeyer-Guerrerio, P.A., Guerrerio, A.L., Oswald, G., Chichester, K., Myers, L., Halushka, M.K., Oliva-Hemker, M., Wood, R.A., and Dietz, H.C. (2013). TGFβ receptor mutations impose a strong predisposition for human allergic disease. Sci. Transl. Med. *5*, 195ra94.
19. Guerrerio, A.L., Frischmeyer-Guerrerio, P.A., Huang, C., Wu, Y., Haritunians, T., McGovern, D.P.B., MacCarrick, G.L., Brant, S.R., and Dietz, H.C. (2016). Increased Prevalence of Inflammatory Bowel Disease in Patients with Mutations in Genes Encoding the Receptor Subunits for TGFβ. Inflamm. Bowel Dis. *22*, 2058–2062.

20. Kotlarz, D., Marquardt, B., Barøy, T., Lee, W.S., Konnikova, L., Hollizeck, S., Magg, T., Lehle, A.S., Walz, C., Borggraefe, I., et al. (2018). Human TGF-β1 deficiency causes severe inflammatory bowel disease and encephalopathy. Nat. Genet. *50*, 344–348.
21. Sobreira, N., Schiettecatte, F., Valle, D., and Hamosh, A. (2015). GeneMatcher: a matching tool for connecting investigators with an interest in the same gene. Hum. Mutat. *36*, 928–930.
22. Loeys, B.L., Schwarze, U., Holm, T., Callewaert, B.L., Thomas, G.H., Pannu, H., De Backer, J.F., Oswald, G.L., Symoens, S., Manouvrier, S., et al. (2006). Aneurysm syndromes caused by mutations in the TGF-beta receptor. N. Engl. J. Med. *355*, 788–798.
23. Jaganathan, K., Kyriazopoulou Panagiotopoulou, S., McRae, J.F., Darbandi, S.F., Knowles, D., Li, Y.I., Kosmicki, J.A., Arbelaez, J., Cui, W., Schwartz, G.B., et al. (2019). Predicting Splicing from Primary Sequence with Deep Learning. Cell *176*, 535–548.e24.
24. Abrams, E.W., and Mullins, M.C. (2009). Early zebrafish development: it's in the maternal genes. Curr. Opin. Genet. Dev. *19*, 396–403.
25. Stainier, D.Y.R., Raz, E., Lawson, N.D., Ekker, S.C., Burdine, R.D., Eisen, J.S., Ingham, P.W., Schulte-Merker, S., Yelon, D., Weinstein, B.M., et al. (2017). Guidelines for morpholino use in zebrafish. PLoS Genet. *13*, e1007000.
26. Mullins, M.C., Hammerschmidt, M., Kane, D.A., Odenthal, J., Brand, M., van Eeden, F.J., Furutani-Seiki, M., Granato, M., Haffter, P., Heisenberg, C.P., et al. (1996). Genes establishing dorsoventral pattern formation in the zebrafish embryo: the ventral specifying genes. Development *123*, 81–93.
27. Tucker, J.A., Mintzer, K.A., and Mullins, M.C. (2008). The BMP signaling gradient patterns dorsoventral tissues in a temporally progressive manner along the anteroposterior axis. Dev. Cell *14*, 108–119.
28. Hammerschmidt, M., and Mullins, M.C. (2002). Dorsoventral patterning in the zebrafish: bone morphogenetic proteins and beyond. Results Probl. Cell Differ. *40*, 72–95.
29. Rossi, A., Kontarakis, Z., Gerri, C., Nolte, H., Hölper, S., Krüger, M., and Stainier, D.Y.R. (2015). Genetic compensation induced by deleterious mutations but not gene knockdowns. Nature *524*, 230–233.
30. Cannaerts, E., van de Beek, G., Verstraeten, A., Van Laer, L., and Loeys, B. (2015). TGF-β signalopathies as a paradigm for translational medicine. Eur. J. Med. Genet. *58*, 695–703.
31. Van Gucht, I., Meester, J.A.N., Bento, J.R., Bastiaansen, M., Bastianen, J., Luyckx, I., Van Den Heuvel, L., Neutel, C.H.G., Guns, P.J., Vermont, M., et al. (2021). A human importin-β-related disorder: Syndromic thoracic aortic aneurysm caused by bi-allelic loss-of-function variants in IPO8. Am. J. Hum. Genet. Published online May 18, 2021. https://doi.org/10.1016/j.ajhg.2021.04.019.

The American Journal of Human Genetics, Volume *108*

Supplemental information

Bi-allelic variants in *IPO8* cause a connective tissue disorder associated with cardiovascular defects, skeletal abnormalities, and immune dysregulation

Alban Ziegler, Rémi Duclaux-Loras, Céline Revenu, Fabienne Charbit-Henrion, Bernadette Begue, Karine Duroure, Linda Grimaud, Anne Laure Guihot, Valérie Desquiret-Dumas, Mohammed Zarhrate, Nicolas Cagnard, Emmanuel Mas, Anne Breton, Thomas Edouard, Clarisse Billon, Michael Frank, Estelle Colin, Guy Lenaers, Daniel Henrion, Stanislas Lyonnet, Laurence Faivre, Yves Alembik, Anaïs Philippe, Bruno Moulin, Eyal Reinstein, Shay Tzur, Ruben Attali, George McGillivray, Susan M. White, Lyndon Gallacher, Kerstin Kutsche, Pauline Schneeberger, Katta M. Girisha, Shalini S. Nayak, Lynn Pais, Reza Maroofian, Aboulfazl Rad, Barbara Vona, Ehsan Ghayoor Karimiani, Caroline Lekszas, Thomas Haaf, Ludovic Martin, Frank Ruemmele, Dominique Bonneau, Nadine Cerf-Bensussan, Filippo Del Bene, and Marianna Parlato

Supplemental Case reports

Cohort

Affected individuals were clinically evaluated in different centers and gathered via GeneMatcher[1]. Each individual or legal guardians gave informed consent for participation in the study. This study was approved by the ethics committees and the institutional review boards at each center.

Family 1- Individual 1, a male, was born to consanguineous parents of Ashkenazi origin. He was referred at age 59 with a putative diagnosis of connective tissue disorder. He had a past history of congenital umbilical hernia, recurrent spontaneous pneumothorax, rectal prolapse and scoliosis. He was disabled by joint hypermobility and had recurrent dislocations of the knees and shoulders. He did not have skin hyperextensibility but he reported bruising easily. Palate, chest and arm span to body height ratio (1.03) were normal. At age 35, his high myopia was complicated by bilateral retinal detachment and at age 45 he developed a bilateral cataract in the absence of lens subluxation. Vascular screening performed at age 59 evidenced a dilatation of both ascending (42mm, Z score +6.79) and abdominal aorta requiring beta-blocker therapy. A mitral valve prolapse as well as dilated and calcified femoral arteries were evidenced. A large cortical cyst (11 cm) of the left kidney was incidentally discovered on CT-scan. He died at age 67 of an unknown cause. **Individual 2**, the youngest sister of individual 1, was referred at age 53 with the putative diagnosis of Marfan syndrome. Like her brother, her medical history was significant for recurrent spontaneous pneumothorax (at age 27 and 31), joint hypermobility with joint dislocation (mainly the elbows), high myopia complicated by retinal detachment at age 17 and bilateral cataract. She also had severe scoliosis, umbilical and spigelian hernias which occurred after abdominal surgery. At age 53, the diameter of the ascending aorta was normal but she had dilatation of sinus of Valsalva (39 mm, Z score +5.23) requiring beta-blocker therapy as well as an abdominal aortic aneurysm. Multiple aneurysms affecting left internal femoral and left popliteal arteries were also present. These aneurysms were associated with peripheral artery disease in lower limbs. At age 53, an ischemic nephropathy consecutive to a thrombosis of the right renal artery and stenosis of the left renal was detected. Palate, chest and arm span to body height ratio were normal. She died at age 65 after surgery for her abdominal aortic aneurysm. Both individuals 1 and 2 were normally intelligent and had no dysmorphic features.

Family 2- Individual 3, a male child was born to consanguineous parents of Indian origin. At 33 weeks of gestation, ultrasonography showed bilateral pelvicalyceal dilatation. He was born at term but was small for gestational age and required neonatal resuscitation for respiratory distress. Birth weight was 2165g (–2SD), length was 50cm (0 SD) and OFC was 35 cm (0 SD). Neonatal echocardiography showed dilatation of heart chambers and ventricular septal defect (6 mm) as well as severe pulmonary arterial hypertension. Bilateral hydroureteronephrosis was present and testes were undescended. He underwent surgery for congenital diaphragmatic hernia and left inguinal hernia at 6 and 15 months respectively. Clinical assessment at 20 months of age evidenced a developmental delay associated with microcephaly (44cm; - 4.4 SD). Dysmorphic features included low set and posteriorly rotated ears, ptosis, down-slanted palpebral fissures, micro-retrognathia, narrow mouth with downturned corners, cleft uvula, curly and hypopigmented hair. In addition, he

had a pectus carinatum, mild arachnodactyly, bilateral eversion of feet, umbilical hernia and hip dysplasia. At echocardiography, the aortic root diameter was measured at 17 mm (Z score +2.19). In addition, he had a perimembranous ventricular septal defect (4 mm), an atrial septal defect (2 mm), as well as a left to right shunt with mild dilatation of left atrium and ventricle. **Individual 4,** his younger brother presented similar clinical features. He had bilateral equinovarus talipes that was evidenced during pregnancy at 35-36 weeks' gestation. Clinical assessment at 24 months of age evidenced motor development delay with normal growth parameters. Echocardiography was normal. Dysmorphic features included micrognathia, small mouth with downturned corners, curly and hypopigmented hair. In addition, he had a pectus carinatum, mild arachnodactyly and umbilical hernia.

Family 3 - Individuals 5 and 6 were born to consanguineous parents of Algerian origin. Both were born at term and presented severe hypotonia and swallowing difficulties from neonatal period. They had both global developmental delay and facial dysmorphic features including bilateral parietal bossing, enlarged nose, micrognathia and hypertelorism. They also had joint hyperlaxity, umbilical hernia and pectus excavatum. In both of them, at age 12 and 14, respectively, brain MRI evidenced bilateral tortuous internal carotids and helicoidal arteriography combined with CT Scan showed enlarged diameters of Valsalva sinus at 32 mm (+2.4SD) and 34mm (+3SD), respectively, as well as pulmonary emphysema and bronchiectasis. **Individual 5**, a girl, also displayed congenital septal defect, severe gastroesophageal reflux (both corrected by early surgery) and pyelo-ureteral duplication. At 4 years, she developed colitis revealed by rectal bleeding and stunted growth. Colonic endoscopy showed pancolitis with mild eosinophilic infiltration. She was treated with corticosteroids and azathioprine; now at 16 years, she remains treated with methotrexate. Her weight and height are currently -2 SD. She also has severe scoliosis treated with physiotherapy and corset. **Individual 6**, a boy, was diagnosed with celiac disease at the age of 3 because of stunted growth, total duodenal villous atrophy, intraepithelial lymphocyte infiltrate, HLA-DQ2 haplotype as well as high titers of serum anti-transglutaminase and anti-endomysium IgG antibodies. He also had nodular gastritis. His growth improved with gluten free diet. At age 12, brain MRI evidenced mild bilateral ventricular dilatation and pituitary hypoplasia. At age 15, his weight and height are -2SD and -1SD of growth standards median respectively. In addition, both siblings have allergic manifestations including asthma and eczema and as well as recurrent pulmonary infections and bronchiectasis. Immunological work-up showed normal lymphocyte counts and phenotype but revealed very low serum IgA (< 0.04g/L, ref:0,45-3.5g/L) contrasting with very high serum IgE (> 1000 kIU/L, ref: <30 IU/L) and IgG (18-28 g/L, ref: <10g/L). Individual 6 has also developed vitiligo.

Family 4- Individual 7, a boy, was born at 36 weeks' gestation after a normal pregnancy to consanguineous parents originating from the United Arab Emirates. He was referred at 12 years of age with the diagnosis of connective tissue disorder. He underwent several surgeries for birth defects including palatal cleft, inguinal hernia and umbilical hernia. Since the neonatal period, he presented with hypotonia, delayed motor development (independent walking was acquired at the age of 9), severe language delay (first words spoken at the age of 6) caused by moderate to severe bilateral conductive hearing loss. He also displayed scoliosis, joint hyperlaxity with multiple dislocations/luxations of large and small joints, skin hyperlaxity associated with mammary

hypoplasia, nail hypoplasia as well as facial dysmorphic features including micrognathia, hypertelorism and proptosis. He had asthma since age 2 and was hospitalized repeatedly for pulmonary infections. Brain MRI and cardiac echocardiography performed at age 7 were considered normal.

Family 5- Individual 8, a male child was born to consanguineous parents of Moroccan origin at 40 weeks of gestation after a normal pregnancy. He had congenital umbilical hernia, bilateral hydroureteronephrosis revealed at 12 months by acute pyelonephritis and developmental delay affecting both motor and language acquisitions. At age 3, he presented digestive symptoms including diarrhea, rectal bleeding and anal fissure associated with stunted growth (-2SD). Endoscopy revealed pancolitis, mild esophageal ulcerations, inflammatory gastritis and duodenitis. Immunological work-up showed transient deficit in IgA (0.07g/L, ref:0,45-3.5g/L), which normalized two years later, high serum IgG (> 15g/L, ref: <10g/L) and IgE (279 kIU/L, ref: <30 IU/L) and hypereosinophilia, that persisted over time. He simultaneously developed allergic symptoms with atopic dermatitis in infancy followed by allergic rhinoconjunctivitis. Now at age 14, he still has high fecal calprotectin (1433 μg/g, ref: <50 μg/g) with Crohn-like inflammation (including microgranulomas) of the colon and ileum and nodular gastritis despite azathioprine and mesalazine and was therefore recently switched to anti-TNF treatment. Severe joint laxity was observed since the age of 3, causing walking difficulties, recurrent pain in the knees and he suffered several spontaneous fractures of the tibia. Beighton score was 8/9 at 9 years when cutaneous laxity with ecchymoses and blue sclera were also noted. At 6 years, echocardiography evidenced moderate dilation of the aortic root at 24 mm (N< 21mm) that was confirmed at the age of 9 (26mm, Z-score +2.63). Pituitary hypoplasia with growth delay (-2.5 SD) and very low serum GH and IGF1 was diagnosed at age 9 requiring a treatment with growth hormone. His weight and height are currently at -2SD of the growth standards median and he has developed mild scoliosis and severe myopia.

Family 6- Individual 9, a woman, was born to consanguineous parents of Arab-Muslim origin. She was referred at age 22 because of dilated aorta and clinical suspicion of a connective tissue disorder. In infancy, she presented with low muscle tone and delayed motor developmental milestones contrasting with normal intellectual, speech and language development. An atrial septal defect was surgically repaired at the age of 1 month. At age 12, an aortic dilatation affecting the aortic root and ascending aorta was diagnosed and treated with beta-blockers. She had recurrent patella dislocation, early osteopenia and hip fracture as well as high myopia without lens dislocation. At age 17, she underwent surgical repair of severe scoliosis. On physical examination, she had marfanoid habitus, her height was 157cm and weight was 36 kg. She had dysmorphic features including exophthalmos, micrognathia, high arched and narrow palate, arachnodactyly, and pectus carinatum. Her skin was normal without abnormal scarring, hyper-extensibility or stretch marks. There was joint laxity especially in the interphalangeal joints, low muscle mass and low fat mass, flat feet and hind foot valgus. Radiological and echographic examination showed lumbosacral dural ectasia, severe scoliosis, aortic root dilatation at sinus of Valsalva (35mm; Z-score +3.4) as well as bilateral tortuosity of the carotid arteries.

Family 7- Individual 10, a girl born to unrelated parents of Australian origin was persistently hypotonic following a Caesarian delivery at term. Her birth weight was 2500g (10th centile). She failed to thrive and needed a fundoplication for reflux with recurrent pneumonia at 9 months of age and surgical patch repair of ventricular and auricular septal defects at 11 months of age. She was assessed in genetics at 17 months of age for failure to thrive (weight and height below the third centile), bilateral positional talipes and delayed motor development. At age 13, she had aortic root dilatation treated with a beta blocker and two forearm fractures following trauma. She had scoliosis with a reduced upper segment to lower segment ratio (0.81), a normal span to height ratio (1.02) and associated short stature (3rd centile) in the setting of delayed pubertal development (Tanner stage 3). She had joint hypermobility (Beighton score 7/9), long fingers with positive thumb and wrist signs, long 2nd and 3rd toes, a high arched palate with a normal uvula, dysplastic teeth, and a flat midface with prominent eyes. Her hypotonia had resolved, she attended a mainstream school and had minor cognitive and fine motor delays. There was no evidence of a generalized bone pathology and her bone density was appropriate for her pubertal stage. At age 14, she had an elbow dislocation and needed a wheelchair for severe hip pain. She required bilateral hip joint replacement for severe hip dysplasia with progressive protrusio acetabulae. She required spinal fixation with anterior lumbar fusion at age 16 of for progressive scoliosis with rib-cage distortion. Her aortic root dilatation had progressed on beta-blocker therapy. Her cardiac anatomy was normal. She was seen more regularly between the age of 24 and her current age of 33 years and clinical diagnoses of Ehlers-Danlos syndrome (EDS) VI or Loeys-Dietz (LDS) syndrome were considered. Her height, weight, head circumference are 150 cm, 57 kg and 55 cm respectively. Her skin feels soft and smooth and is hyperextensible but is not loose and demonstrates normal scarring. She has generalized reduced muscle strength (3-4/5) and experiences chronic joint related pain, in the absence of inflammatory joint changes, and chronic generalized fatigue. She has prominent eyes, shallow orbits, midface retrusion, relative prognathism, dental crowding, gingivitis/ gingival retrusion, a high arched palate and a normal uvula. She has had orthopedic surgery on different occasions for dislocations of one ankle, one knee, one toe and one wrist caused by minor trauma. Painful recurrent subluxations of one shoulder was not improved by surgery. She has also dislocated both thumbs and her temporomandibular joint. She has had recurrent fractures of the metacarpals of one foot and the opposite ankle with minor but proportional trauma. She required abdominal surgery on different occasions for a large anterior abdominal wall hernia that required mesh insertion, for an impacted paraumbilical hernia, and for cholecystitis. She was investigated for gastroparesis and constipation/ decreased colonic transit time. She has always been normotensive and in sinus rhythm. She has stable asymmetrical aortic root dilatation (43mm, Z score +5.29) with aneurysmal dilatation of the right coronary cusp, borderline normal sinotubular diameters, a normal aortic arch, and normal pulmonary arteries with normal pulmonary pressures. She has not had aneurysmal dilatation of her coronary arteries or any medium sized arteries. She has exertional dyspnea and unexplained mild exertional hypoxia with no evidence of cardiac failure nor of significant right to left shunt. She has mild restrictive lung disease and mild asthma. She has moderate myopia requiring glasses, and non-specific retinal changes with no evidence of retinal detachment.

Family 8- Individual 11, a boy born to consanguineous parents of Iranian origin was referred at age 7. He had several congenital defects including umbilical hernia, club feet, bifid uvula and pectus carinatum. He had gradually developed a C-shaped scoliosis and showed mild arachnodactyly but arm spam to height ratio was normal (1.01). His motor development was more delayed (independent walking acquired at 29 months of age) than language acquisition (he spoke his first words at 17 months of age). High myopia without lens subluxation was diagnosed at the age of 3. Due to recurrent abdominal pain, he underwent esophagogastroduodenoscopy at age 3 which showed mild chronic gastritis and duodenitis. Serum immunoglobulins (G, A, M and E) were normal and there was no evidence of hypereosinophilia. Abdominal ultrasound showed a duplicated collecting system of the left kidney with mild hydronephrosis. Vascular screening performed at age 7 evidenced a dilatation of the aortic root (aorta sinuses = 31 mm Z scores+5.15) and floppy mitral valves.

Family 9- Individual 12, a woman, was born to consanguineous parents of Tunisian origin. She was referred at age 24 with the putative diagnosis of EDS. She was a full-term eutrophic baby but had an axial hypotonia that persisted until she was 18 months, bilateral hip dislocation, pes planus and umbilical hernia, that was repaired surgically. Complete hair loss occurred at age 11. She was also diagnosed with celiac disease and presented drug allergies. Her myopia and bilateral cataract required surgery at age 23. Physical assessment at age 24 found facial features evocative of vascular EDS including micrognathia, narrow nose, prominent eyes, and blue sclera. She also had skin fragility with easy bruising, abnormal scarring and skin hyperextensibility. In addition, she had varicose veins of the lower limbs that had appeared at 6 years, joint hypermobility (Beighton score 9/9) without scoliosis as well as complete absence of the permanent dentition. She was normally intelligent. Vascular screening showed carotid artery tortuosity with ectasia of the carotid bulb (15mm). Diameter of the aortic sinus was 41mm (z scores: 4.8).

Supplemental Figures

Figure S1. Additional clinical features of affected individuals.

Whole body pictures of I-3 and I-7 illustrating phenotypic variability in dolichostenomelia.

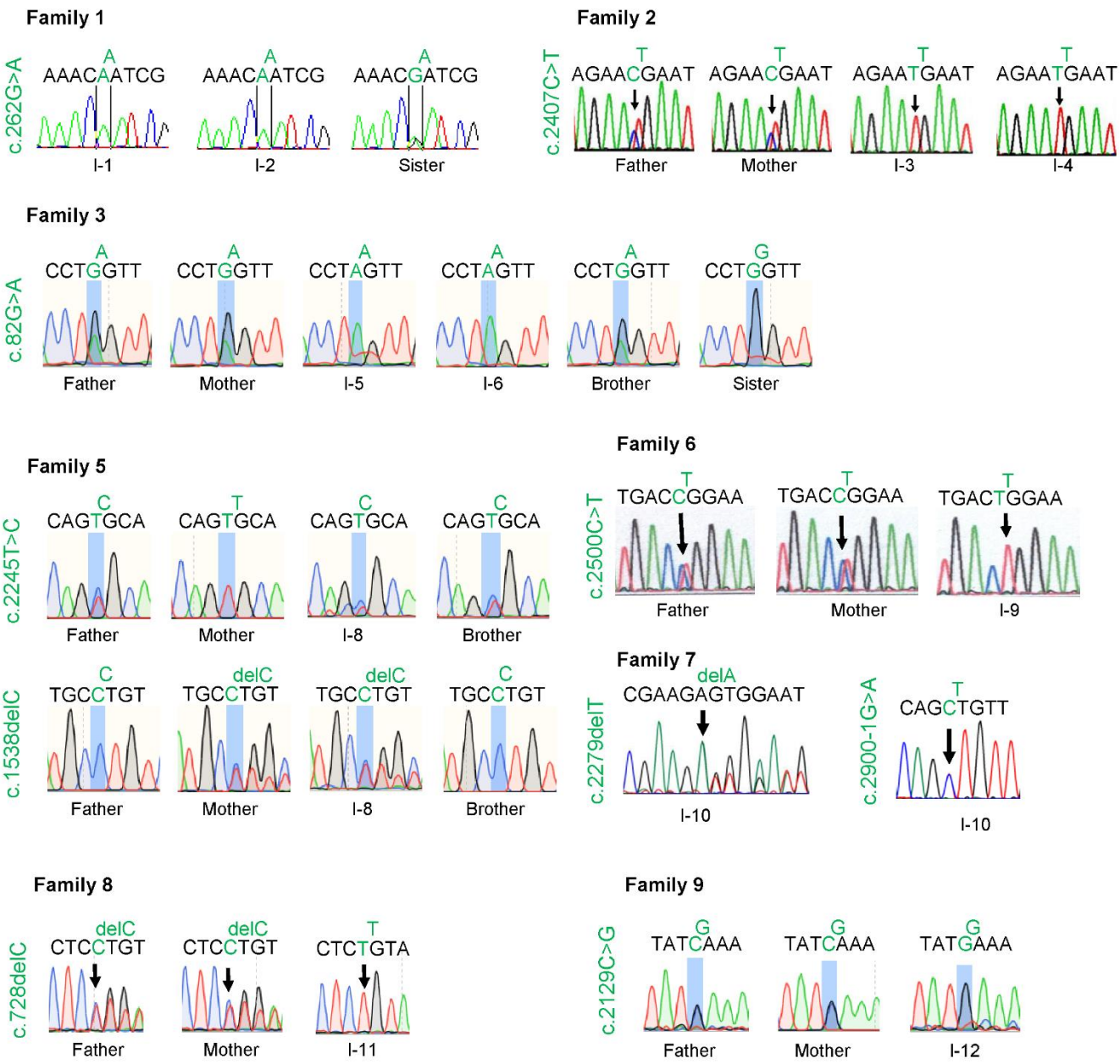

Figure S2. Confirmation of *IPO8* variants by Sanger sequencing.

Sanger tracings in families 1-2-3-5-6-7-8-9.

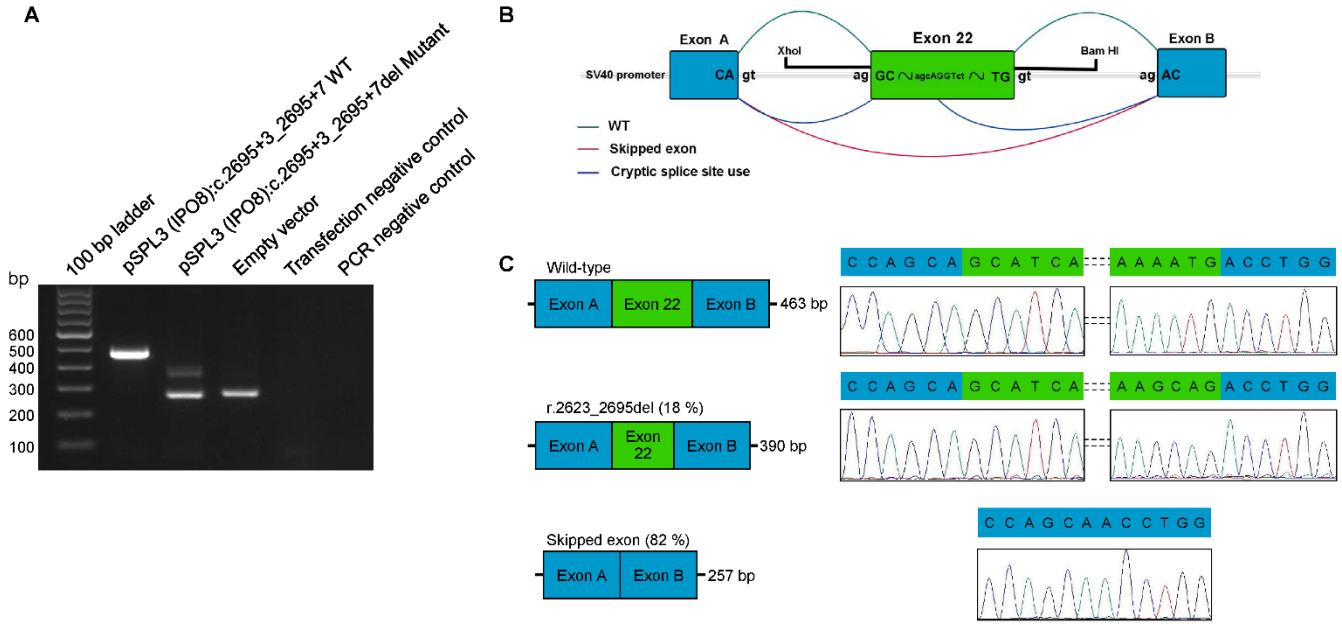

Figure S3. *In vitro* splicing assay of the *IPO8* c.2695+3_2695+7del variant.

(A) cDNA RT-PCR products amplified from constructs following transfection. Wild-type splicing yields a 463 bp product. The mutant amplicon shows two bands, one of which shows skipping of exon 22 (257 bp) while the second weaker band indicates activation of a cryptic donor site (390 bp). Transfection negative and PCR negative controls performed as expected.

(B) Schematic of the pSPL3 exon trapping vector with cloned IPO8 exon 22 (green) with splicing outcomes. Exons A and B (blue) originate from the vector. Wild-type splicing is shown in teal (top). Mutant splicing is depicted in blue (cryptic splice site activation) and red (skipping of exon 22) (bottom).

(C) Electropherograms of the splice junction sites for the wild-type (upper panel), activated cryptic splice site (middle panel, 18% of amplicon pool) and skipped exon 22 (bottom panel, 82% of amplicon pool).

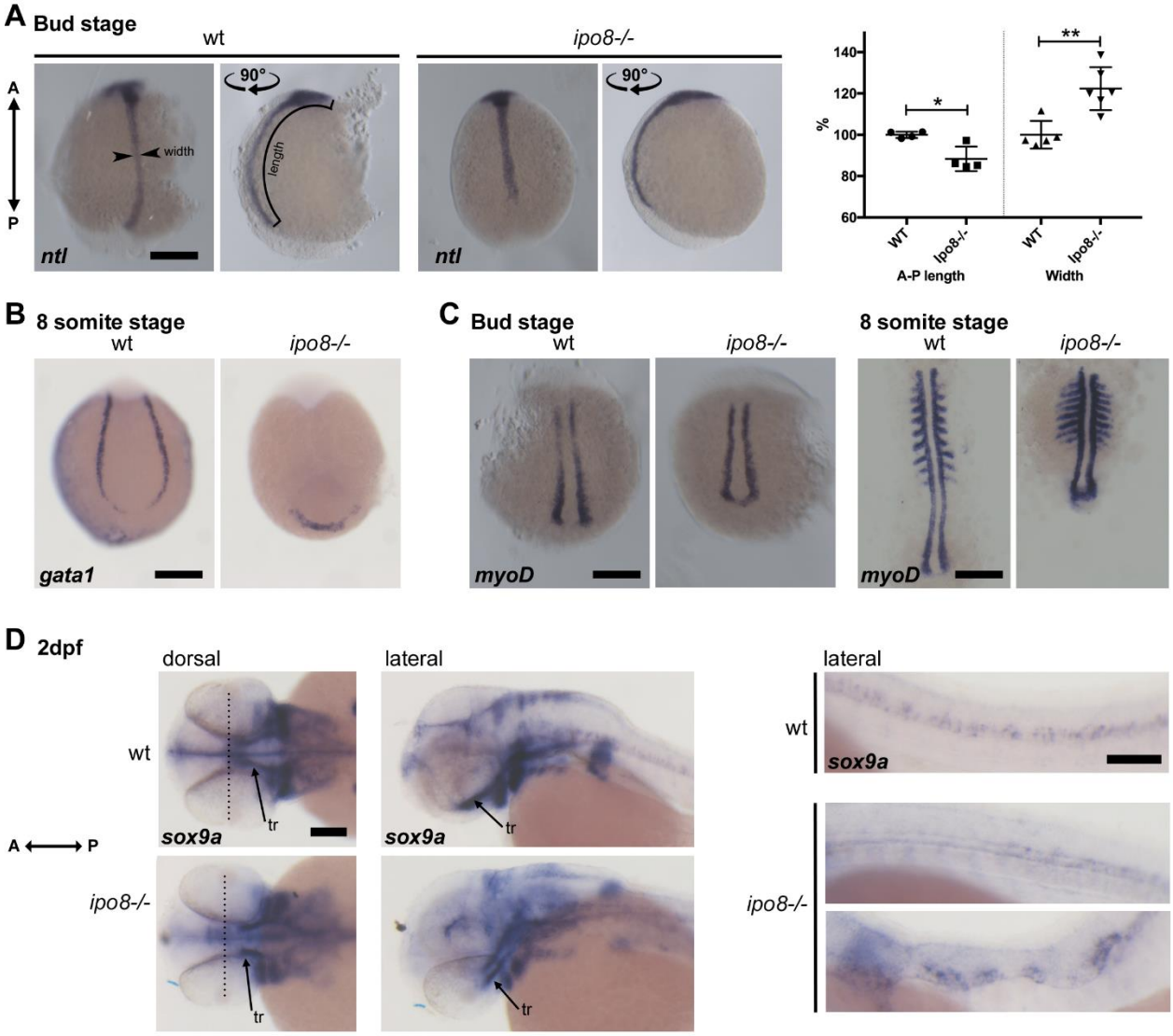

Figure S4: *Ipo8* deficiency causes dorso-ventral patterning defects and skeletal defects in zebrafish.

In situ hybridization pictures of wt and *ipo8*$^{-/-}$ embryos at the indicated stages for the early patterning genes *ntl* (A), *gata1* (B), *myoD* (C) and the chondrogenic precursor marker *sox9a* (D). Penetrance of the dorsalization phenotype is variable: only *ipo8*$^{-/-}$ embryos with strong phenotype are shown. In A, box plots show quantifications of the antero-posterior length and of the width of the ntl stripe. Medians and IQR are shown. P-values are calculated by Mann Whitney test *p<0.05, **p<0,01). A-P, antero-posterior, tr trabecula. In A-C scale bars= 200µm, in D scale bars= 50µm.

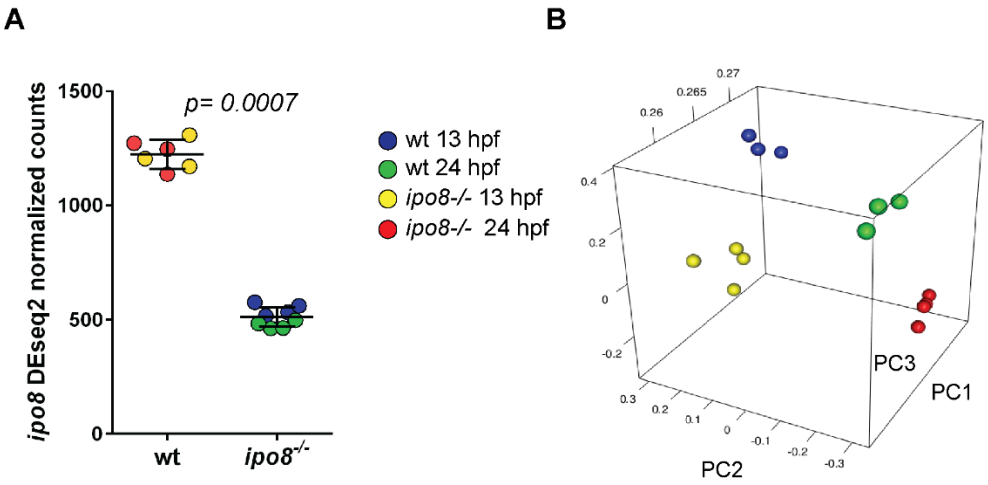

Figure S5: Global analysis of the zebrafish RNA-seq data.

(A) *Ipo8* expression (DESeq2 normalized counts).

(B) Principal component analyses (PCA) of *ipo8*$^{-/-}$ and wt samples at 13 and 24 hpf showing the distribution of the gene profile of each sample. PC1=83.1%, PC2=14.6%, PC3=1.4% on the common modulated genes ($p<0.05$, fold 1.2) between all compared conditions.

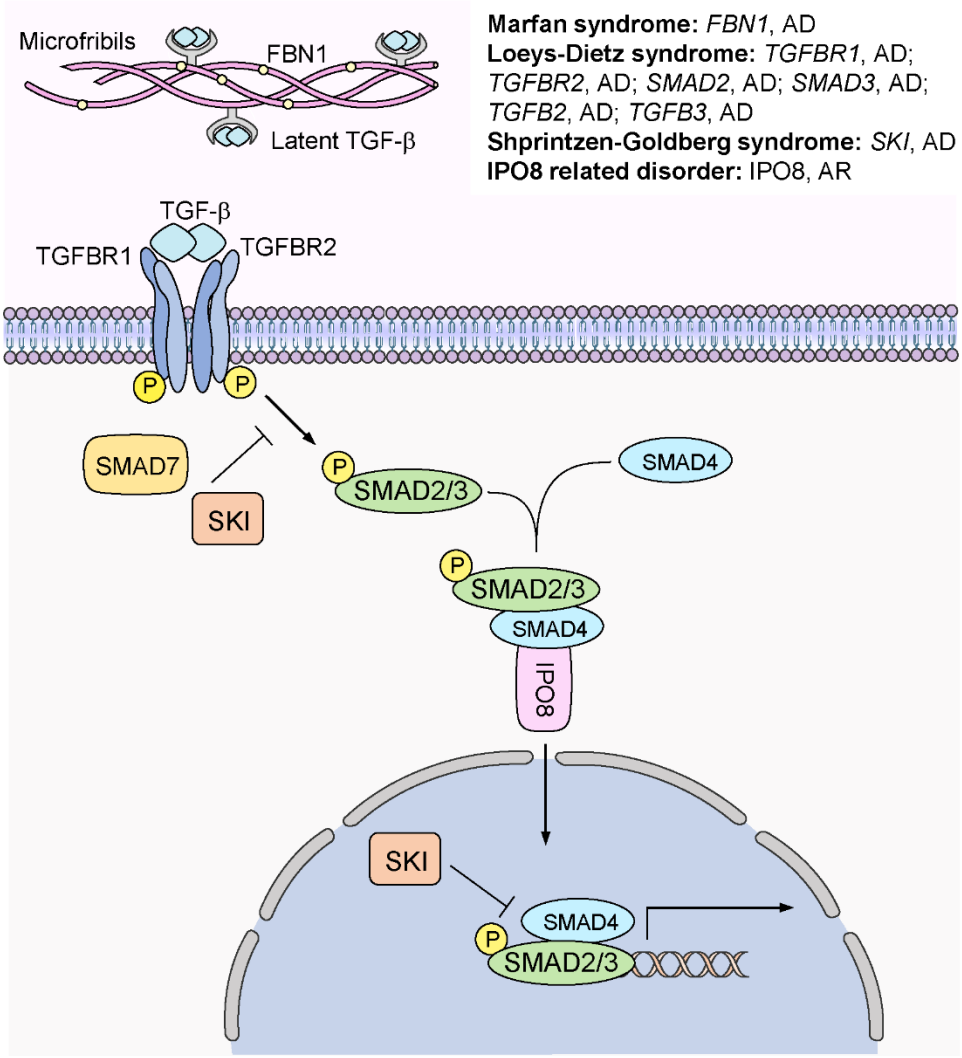

Figure S6: TGF-β signaling via canonical pathway.

In MFS individuals, AD variants in FBN-1, the gene coding for the main component of the extracellular matrix, fibrillin-1, increase the bioavailability of TGF-β ligands. In LDS individuals, AD variants have been reported in TGF-β ligands, TGF-β receptors or R-Smad effectors. In SGS individuals, AD variants have been reported in SKI, which prevents the translocation of R-Smads effectors to the nucleus or their binding to DNA. In IPO8-related disorder, AR variants have been identified in IPO8, the karyopherin which mediates the nuclear transport of the Smad complexes. AD, autosomal dominant, AR, autosomal recessive.

Table S1: Clinical features in MFS, LDS, SGS and IPO8 patients.

Clinical Features		**Marfan**	**Loeys-Dietz**	**Shprintzen-Goldberg**	***IPO8*-related disorders**
Gene(s)		*FBN1*	*TGFBR1/2* *SMAD2/3* *TGFB2/3*	*SKI*	*IPO8*
Mode of inheritance		AD	AD	AD	AR
Heart and blood vessels	Aortic root aneurysm	+++	+++	+	++
	Arterial tortuosity	-	++	+	+
	Early arterial dissection	+	+++	-	-
	Atrial or Ventricular septal defect	-	+	-	++
Skeleton	Craniosynostosis	-	++	+++	-
	Pectus	++	++	++	++
	Scoliosis	++	++	++	++
	Arachnodactyly	+++	++	++	+
	Feet malposition	-	++	++	+
Joint	Hyperlaxity	+	++	++	+++
Facial features	Hypertelorism	-	+	++	+
	Ocular proptosis	-	+	++	++
Ocular	Severe Myopia	++	+	++	++
	Ectopia lentis	+++	-	-	-
Cleft palate/ bifid uvula		-	++	+	+
Hernia		+	+	++	+++
Immune dysregulation		-	+	-	++
Developmental delay		-	-	++ (cognitive and motor delay)	+ (mostly motor delay)
Ureterohydronephrosis		-	-	-	+

+, feature is rare; ++, feature is more commonly present, +++, feature is most commonly present.
−, feature is absent.
AD, autosomal dominant; AR, autosomal recessive.

Supplemental methods

DNA Sequencing

Next generation sequencing was performed on DNA extracted from peripheral blood for all the individuals. Whole Exome sequencing (WES) was performed in all individuals except individuals 4 and 8, for whom targeted next generation sequencing was performed. Sequence validation and segregation analysis of *IPO8* variants was performed on PBMC-derived DNA from individuals 1, 2, 3, 5, 6, 7, 8, 9, 10, 11 and12 by Sanger sequencing. Target enrichment kits, sequencing platforms, family members tested and coverage are detailed below.

Individual	Capture Kit	Sequencing Platform	Family members tested	Average Coverage	Reference
1-2	Twist Human Core Exome Kit (Twist Bioscience, San Francisco, USA)	HiSeq4000 system (Illumina, San Diego, USA)	I-1 and I-2	77x (99.15% > 25x) and 70x (99.5% > 25x) for Individual 1 and 2 respectively	[2]
3-4	Twist Human Core Exome Kit (Twist Bioscience)	NovaSeq 6000 (Illumina)	Trio	178x (99.81x>40x) for Individual 3	[3]
5-6	Agilent Sure Select All Exon V5 (Agilent, Les Ulis, France)	HiSeq2500 HT system (Illumina)	Trio + two healthy siblings	150.8x (97.4% > 30x) and 155.8x (97.7% > 30x) for Individual 5 and 6 respectively	[4]
7	SureSelect Human All Exon V5 kit (Agilent Technologies)	HiSeq 2000 (Illumina)	I-7	113x	[5]
8	Capture Agilent sureselect custom made (Agilent Technologies)	NovaSeq 6000 (Illumina)	I-8	299.6x (99.4% >30x)	[4]
9	TruSeq Exome Enrichment Kit (Illumina)	HiSeq2500 HT system (Illumina)	Trio + one healthy sibling	90x-110x (85% > 20x)	[6]
10	Nextera exome capture kit (Illumina)	HiSeq_X_10 (Illumina)	Trio	80% >20x	[7]
11	Nextera Rapid Capture Enrichment library preparation kit (Illumina)	NextSeq 500 (Illumina)	Trio	27.1x (67.8% >10x)	[8]
12	Xgen-exome-research-panel (Integrated DNA technologies, Leuven, Belgium)	NextSeq 550 (Illumina)	Trio	115x (97.5% >30x)	[9]

Cell Culture

Primary fibroblasts derived from skin biopsy from individuals 2, 5, 9 and four healthy individuals (controls) were cultured in Dulbecco's modified Eagle medium (Gibco, Thermo Fisher Scientific, Villebon sur Yvette, France) supplemented with 10% fetal bovine serum (Gibco) and penicillin-streptomycin (Gibco). EBV-B cells derived from individuals 5, 6 and 8 were cultured in RPMI medium (Gibco) supplemented with 10% fetal bovine serum (Gibco) and penicillin-streptomycin (Gibco).

Western blot

Total proteins were lysed in RIPA buffer (Sigma-Aldrich, Saint-Quentin Fallavier, France) supplemented with 1X proteinase inhibitor cocktail mix (Roche, Sigma-Aldrich). Protein concentration was measured by Bradford protein assay (Biorad, Marnes-la-Coquette, France). Equal amounts of proteins in Laemmli buffer (Biorad) were separated by SDS–PAGE, transferred to a polyvinylidene difluoride membrane (Biorad), blocked with 5% milk protein in TBST (0.5% Tween, Biorad) and probed with primary antibodies. The membranes were washed with TBST and incubated with appropriate secondary antibodies. Primary antibodies directed against IPO8 (#398854, 1:100, Santa Cruz, Dallas, USA), GAPDH (#14C10, 1:1000, Cell Signaling Technology, Leiden, The Netherlands). Secondary peroxidase–conjugated anti-rabbit and anti-mouse (1:1000, Cell Signaling Technology) were used. Specific protein bands were visualized using an ECL advanced Western blotting detection kit (GE Healthcare, Amersham, UK). The immunoblot was repeated at least twice for each patient.

Zebrafish (*Danio rerio*) husbandry and mutant generation

Wild-type Tupfel long fin zebrafish strains were used and raised according to standard protocols. All animal procedures were performed in accordance with French and European Union animal welfare guidelines with protocols approved by Sorbonne Université and Institut Curie (APAFIS#21323-2019062416186982 and APAFIS#6031-2016070822342309). To generate the *ipo8* mutant, the CRISPR/Cas9 technology was used. The crRNA (with *ipo8* exon4 specific sequences: sg5 AGTCGCAGAACAGTGGCAGC and sg6 TAAAGCATGATTTTCCTGGC) and tracrRNA sequences were ordered at IDT (Leuven, Belgium). Oligonucleotides were annealed according to the manufacturer's instructions at 45µM each in 20mM Hepes-NaOH pH 7.5, 150mM KCl. 1µL of the annealed sgRNA (45µM) was mixed with 1µL of Cas9 protein (30µM) and injected in one cell stage embryos [10]. Injected embryos were grown to adulthood and crossed with WT fish to identify founders. Pools of 20 embryos per clutch were lysed in NaOH 50mM at 95°C for at least 30min. PCR was performed on lysates to amplify the genomic region targeted by the sgRNA with primers forward 5'-GTCCATAAGGCAAGTCACAATGTTT-3' and reverse 5'-AAGAGAGTCAAAAGTGTCGTGTTTC- 3' using Phusion High-Fidelity DNA polymerase (Thermo Fisher Scientific). The amplicons were run on a 3% agarose gel to identify deletions in the targeted region and to select the corresponding founder fish. Deletions were confirmed by sequencing (GATC biotech) and sequences were analyzed using Geneious [11] to select mutations inducing early stop codon. After selection of the founder, genotyping of the line was performed by PCR on fin clips with the same primers.

Zebrafish imaging and quantifications

For live-imaging, embryos were anaesthetized in 0.02% MS-222 and immobilized in 1% low melting point agarose. To visualize endothelial cells *in vivo,* the *ipo8* mutant line was crossed with Tg*(kdrl:Hsa.HRAS-mCherry)s916*. Live imaging was performed on a Zeiss LSM 780 confocal.

In situ hybridization

In situ hybridizations (ISH) were performed on embryos fixed in freshly made 4% paraformaldehyde (PFA) overnight at 4°C and stored in 100% methanol at -20°C. After rehydration, embryos were treated with proteinase K (20 µg/ml, Roche) at RT depending on their stage and fixed again in 4% PFA at RT for 20min. Digoxigenin-labelled antisense and sense RNA probes were synthesized by *in vitro* transcription using DIG-labelled UTP according to the manufacturer's instructions (DIG RNA labelling kit, Roche). Anti-DIG antibody conjugated to alkaline phosphatase allowed detection of hybridized riboprobes according to the manufacturer's instructions (Roche). DNA for probe synthesis was amplified from zebrafish genomic DNA using the following primers (*ntl,* Fwd: ATCATCTCCTTAGCGCCGTG, Rev: ATTGAACTGAGGAGGGCTGC; *myoD,* Fwd: CCCTTGCTTCAACACCAACG, Rev: GACAGATCCCTCATGCGGAG; *gata1,* Fwd: CAGGCTCCAGGAAGTCCTG, Rev: CACTAGTGTGGGCATCATGCC; *sox9a,* Fwd: CCAGCAAAAACAAGCCGCAC, Rev: CTGCCGTTTTGGGGTTTGGT) and transcribed *in vitro* according to the manufacturer's instructions (DIG RNA labelling kit, Roche). Imaging was performed on a Zeiss Discovery V20 stereomicroscope using the ZEN software.

Immunohistochemistry

80% epiboly embryos were fixed overnight at 4°C in 4% PFA and incubated in blocking buffer for at least 1h (10%FCS, 1%DMSO, 0.1%Tween in PBS). Embryos were incubated for 6h at RT with the anti-Phospho-Smad1(Ser463/465)/Smad5(Ser463/465)/Smad9(Ser465/467) Rabbit mAb (clone D5B10, #13820, Cell Signaling Technology) at a dilution of 1:100 in 1%FCS, 0.1%DMSO, 0.1%Tween in PBS, followed by overnight incubation at 4°C with Goat anti-rabbit Alexa Fluor488 antibody (1:400 in previous buffer, A27034, Thermo Fisher Scientific), phalloidin-Alexa Fluor 568 probe (1:40, A12380, Thermo Fisher Scientific) and Dapi (D1306, Thermo Fisher Scientific). After mounting in 1% low melting point agarose, images of the ventral sides were acquired on a Zeiss LSM 780 confocal. For quantifications of the ratio of cytoplasmic over nuclear signal, image segmentation was performed on the Dapi channel to create a binary mask used to quantify pSmad1/5/9 nuclear signal, using ImageJ. The binary image of segmented nuclei was subtracted from the pSmad1/5/9 image to quantify cytoplasmic signal.

Zebrafish RNA extraction and sequencing

Triplicates of 60 embryos were lysed in 1mL trizol (Invitrogen, Thermo Fisher Scientific) and mixed with a pestle (5min at RT) and RNA was extracted according the manufacturer. RNA pellet was dissolved in 20uL RNAse free water, treated with DNAse (TURBO DNA-free Kit, Thermo Fisher Scientific) for 30 min at 37°C, cleaned up (Qiagen RNA clean up kit, Qiagen, Venlo, The Netherlands) and resuspended in 30uL. RNA quality was assessed using RNA Screen Tape 6000 Pico LabChips with the Tape Station (Agilent Technologies) and the RNA concentration was measured by spectrophotometry using the Xpose (Trinean, Ghent, Belgium). RNAseq libraries were prepared

starting from 1 µg of total RNA using the Universal Plus mRNA-Seq kit (NuGen Technologies Inc. San Carlos, USA) as recommended by the manufacturer. The oriented cDNA produced from the poly-A+ fraction was sequenced on a HiSeq2500 from Illumina (Paired-End reads 130 bases + 130 bases). A total of ~70 millions of passing filter paired-end reads were produced per library. FASTQ files were mapped to the ENSEMBL Zebrafish (GRCz11) reference using Hisat2 and counted by *featureCounts* from the Subread R package. Read count normalizations and groups comparisons were performed by three independent and complementary statistical methods: Deseq2, edgeR, LimmaVoom. Flags were computed from counts normalized to the mean coverage. All normalized counts <20 were considered as background (flag 0) and >=20 as signal (flag=1). P50 lists used for the statistical analysis regroup the genes showing flag=1 for at least half of the compared samples. The results of the three methods were filtered at pvalue<=0.05 and folds 1.2/1.5/2 compared and grouped by Venn diagram. Cluster analysis was performed by hierarchical clustering using the Spearman correlation similarity measure and ward linkage algorithm. Functional analyses were carried out using Ingenuity Pathway Analysis (IPA, Qiagen). Heat maps were made with the R package ctc: Cluster and Tree Conversion and imaged by Java Treeview software.

Statistical Analysis

Data were analyzed using GraphPad Prism software (GraphPad Software, San Diego, CA). P value ≤ .05 was considered significant. The test used in each set of experiment is described in the corresponding figure legends.

References

1. Sobreira, N., Schiettecatte, F., Valle, D., and Hamosh, A. (2015). GeneMatcher: a matching tool for connecting investigators with an interest in the same gene. Hum. Mutat. *36*, 928–930.

2. Colin, E., Daniel, J., Ziegler, A., Wakim, J., Scrivo, A., Haack, T.B., Khiati, S., Denommé, A.-S., Amati-Bonneau, P., Charif, M., et al. (2016). Biallelic Variants in UBA5 Reveal that Disruption of the UFM1 Cascade Can Result in Early-Onset Encephalopathy. Am. J. Hum. Genet. *99*, 695–703.

3. Harms, F.L., Parthasarathy, P., Zorndt, D., Alawi, M., Fuchs, S., Halliday, B.J., McKeown, C., Sampaio, H., Radhakrishnan, N., Radhakrishnan, S.K., et al. (2020). Biallelic loss-of-function variants in TBC1D2B cause a neurodevelopmental disorder with seizures and gingival overgrowth. Hum. Mutat. *41*, 1645–1661.

4. Charbit-Henrion, F., Parlato, M., Hanein, S., Duclaux-Loras, R., Nowak, J., Begue, B., Rakotobe, S., Bruneau, J., Fourrage, C., Alibeu, O., et al. (2018). Diagnostic Yield of Next-generation Sequencing in Very Early-onset Inflammatory Bowel Diseases: A Multicentre Study. J. Crohn's Colitis *12*, 1104–1112.

5. Thevenon, J., Duffourd, Y., Masurel-Paulet, A., Lefebvre, M., Feillet, F., El Chehadeh-Djebbar, S., St-Onge, J., Steinmetz, A., Huet, F., Chouchane, M., et al. (2016). Diagnostic odyssey in severe neurodevelopmental disorders: toward clinical whole-exome sequencing as a first-line diagnostic test. Clin. Genet. *89*, 700–707.

6. Laitman, Y., Tzur, S., Attai, R., Tirosh, A., and Friedman, E. (2020). Germline variant in REXO2 is a novel candidate gene in familial pheochromocytoma. Genet. Res. (Camb). *102*, e3.

7. Ansar, M., Chung, H., Al-Otaibi, A., Elagabani, M.N., Ravenscroft, T.A., Paracha, S.A., Scholz, R., Abdel Magid, T., Sarwar, M.T., Shah, S.F., et al. (2019). Bi-allelic Variants in IQSEC1 Cause Intellectual Disability, Developmental Delay, and Short Stature. Am. J. Hum. Genet. *105*, 907–920.

8. Lekszas, C., Foresti, O., Raote, I., Liedtke, D., König, E.-M., Nanda, I., Vona, B., De Coster, P., Cauwels, R., Malhotra, V., et al. (2020). Biallelic TANGO1 mutations cause a novel syndromal disease due to hampered cellular collagen secretion. Elife *9:e51319.*

9. Wang, V.G., Kim, H., and Chuang, J.H. (2018). Whole-exome sequencing capture kit biases yield false negative mutation calls in TCGA cohorts. PLoS One *13*, e0204912.

10. Albadri, S., Del Bene, F., and Revenu, C. (2017). Genome editing using CRISPR/Cas9-based knock-in approaches in zebrafish. Methods *121–122*, 77–85.

11. Kearse, M., Moir, R., Wilson, A., Stones-Havas, S., Cheung, M., Sturrock, S., Buxton, S., Cooper, A., Markowitz, S., Duran, C., et al. (2012). Geneious Basic: An integrated and extendable desktop software platform for the organization and analysis of sequence data. Bioinformatics *28*, 1647–1649.